Mathematical Geology, Vol. 25, No. 2, 1993

The Fourier Integral Method: An Efficient Spectral Method For Simulation of Random Fields[1]

E. Pardo-Igúzquiza[2] and M. Chica-Olmo[2]

The Fourier Integral Method (FIM) of spectral simulation, adapted to generate realizations of a random function[3] in one, two, or three dimensions, is shown to be an efficient technique of non-conditional geostatistical simulation. The main contribution is the use of the fast Fourier transform for both numerical calculus of the density spectral function and as generator of random finite multidimensional sequences with imposed covariance. Results obtained with the FIM are compared with those obtained by other classic methods: Shinozuka and Jan Method in 1D and Turning Bands Method in 2D and 3D, the points for and against different methodologies are discussed. Moreover, with the FIM the simulation of nested structures, one of which can be a nugget effect and the simulation of both zonal and geometric anisotropy is straightforward. All steps taken to implement the FIM methodology are discussed.

KEY WORDS: spectral generator, geostatistical simulation, spectral density, amplitude spectrum, phase spectrum, discrete Fourier transform, fast Fourier transform, anisotropic covariance.

INTRODUCTION

The most widespread method in the area of geostatistics for the generation of realizations of a multidimensional stationary random function has been the Turning Bands Method (Matheron, 1973; Journel, 1974). The most interesting practical aspect of this method is that only one-dimensional generators are necessary, which are mathematically more simple than the multidimensional models.

As is well known, the Turning Bands Method (TBM) simplifies multidimensional simulations from one-dimensional simulations along lines that are homogeneously distributed over the space to be simulated. The most important relations are those that link the function of one-dimensional covariance on the lines and the objective covariance (Matheron, 1973). In 2D

[1]Accepted 16 March 1992; received 16 December 1991.

[2]Department of Geodynamics/IAGM, Avda. Fuentenueva s/n, Facultad de Ciencias, University of Granada, Granada, Spain.

[3]Random function, random field and stochastic process are considered as synonymous in this paper.

0882-8121/93/0200-0177$07.00/1

$$\int_0^r \frac{C_1(s)}{(r^2 - s^2)^{1/2}}\, ds = \frac{\pi}{2} C_2(r)$$

in 3D

$$C_1(r) = \frac{d}{dr}[rC_3(r)]$$

$C_1(.)$: one-dimension al covariance on the lines, $C_2(.)$: two-dimensional isotropic covariance in 2D, and $C_3(.)$: three-dimensional isotropic covariance in 3D.

In the frequency domain the equivalent relations between the respective functions of spectral density are obtained (Mantoglou, 1987; Christakos, 1987). In 2D

$$S(\omega) = \pi\omega S(\omega)$$

In 3D

$$S(\omega) = 2\pi\omega^2 S(\omega)$$

$S_1(.)$: one-dimensional spectral density function, $S_2(.)$: spectral density function with radial symmetry, $S_3(.)$: spectral density function with spherical symmetry, and ω: angular frequency.

Depending on the dimensionality of the problem (2D or 3D) and the type of one-dimensional generator that we wish to use (spatial or spectral), it is necessary to solve one of the four previous equations, which is more or less simple depending on the covariance model to be simulated.

Mantoglou and Wilson (1982) have shown how the TBM is particularly efficient if used as a one-dimensional generator with the Shinozuka and Jan (1972) spectral method. The generator is expressed as a series of cosine functions the amplitude of which is modulated by the spectral density function:

$$z(x) = 2 \sum_{k=1}^{M} [S(\omega_k)\Delta\omega]^{1/2} \cos(\omega_k' x + \phi_k)$$

$z(x)$: simulated value at the location x, $S(.)$: spectral density function, $\omega_k = (k - 0.5)\,\Delta\omega$: frequency of the kth harmonic, $\Delta\omega = \Omega/M$: discretization interval of the frequency, M: number of harmonics, Ω: maximum spectral frequency, $\omega_k' = \omega_k + \delta\omega$, and $\delta\omega$: small random frequency added to avoid periodicities. The main disadvantage of this method is that the simulated covariance is periodic (Mantoglou and Wilson, 1982):

$$C(h) = 2\frac{\Omega}{M} \sum_{k=1}^{M} S(\omega_k) \cos(\omega_k h)$$

with period $T = 4\pi M/\Omega$. With a fixed maximum spectral frequency (Ω) the

period can be longer if we increase the number of harmonics M, but this implies a greater time of calculus which may not be admissible. Moreover, the spectral density function must be known over a finite set of angular frequencies, which must be evaluated analytically or by numerical methods:

$$\{\omega_k = (k - 0.5)\Delta\omega \quad k = 1, \cdots, M\}$$

Faced with the difficulties of the previous methods makes it necessary to opt for a more general method. The method proposed, although used before by other authors (Bormang et al., 1984), has had important particularities introduced with an important gain in efficiency as will be shown.

FOURIER INTEGRAL METHOD

First at all, it is remarkable that although a theory can be established for infinite and continuous random fields, in practice our aim is to generate realizations of a finite and discrete random function, i.e., a finite set of values located on a grid, so only finite discrete processes are considered in the discussion. Moreover, let the stochastic process to be a real-valued process, which cover the vast majority of processes in Earth Sciences. Additionally, the process is second-order stationary with zero-mean and normalized unity variance, then correlation function and covariance function coincide. Finally, for simplicity in notation, discussion is made on a one-dimensional case; particularities to implement the method in 2D and 3D will be noted.

Any discrete stochastic process $Z(k)$ which is second order stationary can be expressed by its spectral representation as follows (Cox and Miller, 1968):

$$Z(k) = \int_{-\pi}^{\pi} e^{i\omega k} d\mathfrak{U}(\omega)$$

this is, as integrals of stochastic processes of a continuous parameter ω.

For a discrete process measured at unit intervals ($\Delta x = 1$) there is no loss of generality in restricting ω to the range $(-\pi, \pi)$. Variation at frequencies higher than π (Nyquist frequency $= \pi/\Delta x$) cannot be distinguished from variation at a corresponding frequency in $(-\pi, \pi)$ (Chatfield, 1991).

For a real-valued process the spectral representation can be written:

$$Z(k) = \int_0^{\pi} \cos(k\omega)\, d\mathfrak{U}_1(\omega) + \int_0^{\pi} \sin(k\omega)\, d\mathfrak{U}_2(\omega)$$

These processes $\{d\mathfrak{U}_1(\omega), d\mathfrak{U}_2(\omega)\}$ are essentially the limits of the integrals of the cosine and sine transforms (Anderson, 1971):

$$\sum_k z(k) \cos(k\omega)$$

$$\sum_k z(k) \sin(k\omega)$$

Second-order properties of the processes are specified by the spectral density function $S(\omega)$ (Anderson, 1971):

$$E[d\mathfrak{U}_1(\omega)] = E[d\mathfrak{U}_2(\omega)] = 0$$

$$E[d\mathfrak{U}_1(\omega_2) - d\mathfrak{U}_1(\omega_1)]^2 = E[d\mathfrak{U}_2(\omega_2) - d\mathfrak{U}_2(\omega_1)]^2 = \int_{\omega_1}^{\omega_2} S(\omega)\, d\omega$$

$$\text{Cov}\,[d\mathfrak{U}_1(\omega), d\mathfrak{U}_2(\omega)] = E[d\mathfrak{U}_1(\omega)\, d\mathfrak{U}_2(\omega)] = 0$$

$$\text{Var}\,[Z(k)] = \int_{-\pi}^{\pi} S(\omega)\, d\omega$$

$0 \leq \omega_1 \leq \omega_2 \leq \pi$, $E[.]$: mathematical expectation, Cov[.]: covariance, Var[.]: variance, and $S(.)$: spectral density function. On the other hand, the so-called Wiener–Khintchine theorem states that any stationary process has a covariance function $C(h)$ of the form (Anderson, 1971):

$$C(h) = \int_{-\pi}^{\pi} S(\omega) e^{i\omega h}\, d\omega$$

$i = (-1)^{1/2}$, and $S(.)$: spectral density function. And conversely, given a function representable by the last equation, there exists a stationary process with $C(h)$ as covariance (Cox and Miller, 1968). Both functions, covariance and spectral density, contain the same information but express this in different ways.

The two possible interpretations of the spectral density function $S(\omega)$ are given as follows. First, it gives the proportion of the variance of $Z(k)$ contributed by the components in the range $(\omega, \omega + \Delta\omega)$, i.e., gives the probabilistic properties of the components in a Fourier analysis of the process itself (Cox and Miller, 1968). Second, it gives directly the components in a Fourier analysis of the correlation function.

In practice, we can obviate stochastic integrals and simply regard $Z(k)$ as a linear combination of orthogonal sinusoidal terms (Chatfield, 1991).

We construct a model of the discrete random field which is a linear combination of sines and cosines that have, in general, random phases and random amplitudes. But in our case the amplitudes are important and the phases are of no interest. The sum of the mean squared amplitudes of the frequencies in a given interval is equal to the sum of values of the spectral density function in this interval, as is known from spectral analysis.

As is well known by Fourier analysis, a sequence $z(k)$ of N points can be transformed into a finite set of Fourier coefficients (Chatfield, 1991):

$$z(k) = \sum_{j=0}^{N-1} [a_j \cos(2\pi jk/N) + b_j \sin(2\pi jk/N)]$$

$\{k = 0, \ldots, N-1\}$, N: number of points of the sequence.

$$a_j = \frac{1}{N} \sum_{k=0}^{N-1} z(k) \cos(2\pi jk/N)$$

$$b_j = \frac{1}{N} \sum_{k=0}^{N-1} z(k) \sin(2\pi jk/N)$$

$\{j = 0, \ldots, N-1\}$.

Another way of representing the finite discrete sequence is as a complex exponential Fourier series (Hsu and Mehra, 1973):

$$z(k) = \sum_{j=0}^{N-1} A(j) e^{i2\pi kj/N}$$

$i = (-1)^{1/2}$, and $\{k = 0, \ldots, N-1\}$. Where:

$$A(j) = |A(j)| e^{-i\varphi(\omega)}$$

Coefficients $A(j)$ are related to a_j, b_j coefficient by the equations:

$$|A(j)| = \sqrt{a_j^2 + b_j^2}$$

$$\varphi(\omega) = \tan^{-1}(-b_j/a_j)$$

Discrete amplitude spectrum is the representation of amplitude $|A(j)|$ vs. frequency $2\pi j/N$ and phase spectrum is the graph of phase $\varphi(j)$ vs. frequency $2\pi j/N$.

The Parseval–Rayleigh theorem stated that the sum of squared amplitudes is equal to the total power of $\{z(k), k = 0, \ldots, N-1\}$ that can be identified with the variance (Bracewell, 1986):

$$\sum_{j=0}^{N-1} |A(j)|^2 = \frac{1}{N} \sum_{k=0}^{N-1} |z(k)|^2 = \sigma^2$$

σ^2: variance of the sequence $\{z(k), k = 0, \ldots, N-1\}$. The discrete amplitude spectrum can be related directly to the discrete spectral amplitude (Chatfield, 1991):

$$|A(j)|^2 = S(j)$$

$\{j = 0, \ldots, N-1\}$, $|A(j)|$: amplitude spectrum, and $S(j)$: spectral density. This result is also obtained directly from the theorem of the Fourier transform of the correlation function (Bracewell, 1986):

$$C(h) \leftrightarrow |A(j)|^2$$

$\leftrightarrow$: Fourier transform pair.

And, by definition, the spectral density function is the Fourier transform of the covariance function:

$$C(h) \leftrightarrow S(\omega)$$

The spectral density function is an even function:

$$S(j) = S(-j)$$

then

$$|A(j)| = |A(-j)|$$

Figure 1 shows, in diagram form, the information given in the previous paragraphs.

Then, the amplitude spectrum cannot be random but it can be related to the spectral density which depends on the covariance model that we wish to impose on the realization.

The phase spectrum does not affect the covariance structures, then it can be taken at random from a uniform distribution between 0 and 2π:

$$\varphi(j) \sim U(0, 2\pi)$$

$U(0, 2\pi)$: uniform distribution between 0 and 2π. In this way we construct the complex Fourier coefficients:

$$A(j) = |A(j)|e^{-i\varphi(j)}$$

$$A(j) = |A(j)| \cos \varphi(j) - i\,|A(j)| \sin \varphi(j)$$

Real part: $$R(j) = |A(j)| \cos \varphi(j)$$

Imaginary part: $$I(j) = |A(j)| \sin \varphi(j)$$

$$A(j) = R(j) - iI(j)$$

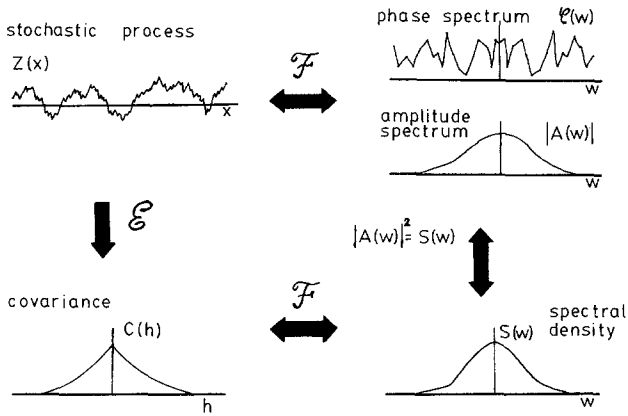

Fig. 1. Basic relations among stochastic process, covariance function, spectral density function and amplitude spectrum. $\mathcal{E}$: estimation, $\mathcal{F}$: Fourier transform.

The Fourier transform of a real function is an hermitian function (Bracewell, 1986); then coefficients $A(j)$ must be hermitian, this is even real part:

$$R(j) = R(-j)$$

and odd imaginary part:

$$I(j) = -I(-j)$$

By calculating the inverse Fourier transform of the complex coefficients $A(j)$, the discrete finite realization $\{z(k), k = 0, \ldots, N-1\}$ is obtained with the specified covariance model:

$$z(k) = \sum_{j=0}^{N-1} A(j) e^{i2\pi jk/N}$$

$k = 0, \ldots, N-1$. If the number of points N is to the power of two, the inverse discrete Fourier transform can be rapidly and efficiently computed with the fast Fourier transform (FFT).

METHODOLOGY

The aim is to generate different realizations of a random field with an imposed model of covariance function. First of all, we must define the characteristics of the field to simulate:

Dimensionality	1D	2D	3D
Number of points	N_1	N_1, N_2	N_1, N_2, N_3
Point interdistance	Δx	$\Delta x, \Delta y$	$\Delta x, \Delta y, \Delta z$

N_1, N_2, and N_3 have to be a multiple of two in order to apply FFT algorithms.

Second, we must define the correlation structure defined by the covariance function:

Nugget effect?

Number of nested structures?

For each structure: Type of covariance model?

Sill?

Range?

Zonal anisotropy? (not applicable in 1D)

Geometric anisotropy? (not applicable in 1D)

The steps for the simulation are proposed as follows and are shown in diagram form in Fig. 2.

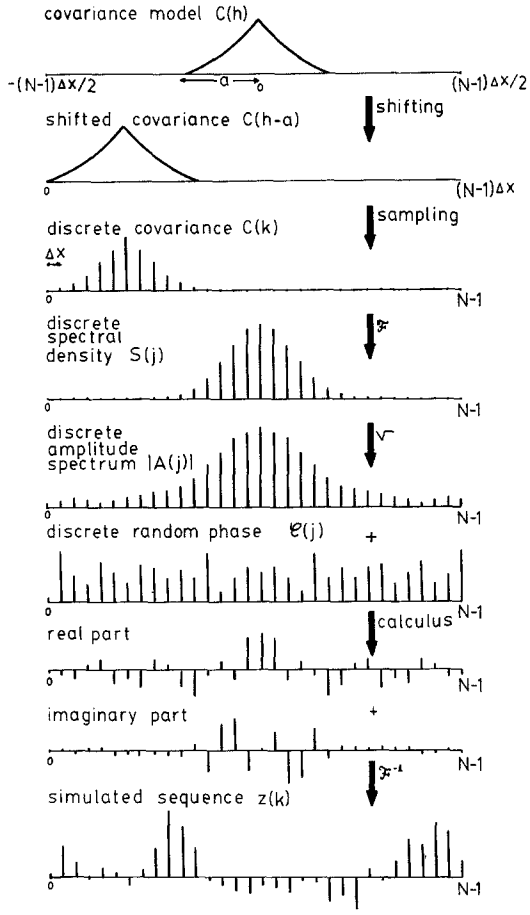

Fig. 2. Steps in simulation process. $\mathcal{F}$: Fourier transform, $\mathcal{F}^{-1}$: inverse Fourier transform.

Step 1: Sampling the Covariance

Sampling the covariance model in one- two- or three dimensions, in the directions of the axes of the cartesian coordinates, to obtain the sequence of the sampled covariance. For example, in 2D we obtain the sequence:

$$\{C(k_1, k_2);\ k_1 = 0, \ldots, N_1 - 1;\ K_2 = 0, \ldots, N_2 - 1\}$$

The covariance model can be any permissible model of covariance in the correspondent dimension. Moreover, it can have nested structures, one of which may be a nugget effect or the covariance may be anisotropic.

The length of sampling is equal to the length of the field to simulate as can be seen in Fig. 2a for 1D. For this purpose the covariance is shifted as indicated in Fig. 2b. This is done because in the equations of the discrete Fourier transform we work with the assumption that the function to be Fourier transformed has bounded support over $[0, N_1\Delta x]$ (in 1D), that is, zero for $x < 0$ (Weaver, 1989). This is the case of the covariance function which, in particular, is an even function $C(h) = C(-h)$, then the covariance is shifted before sampling a value which, at least, is equal to the length of correlation of the covariance model. We can deduce that the length of the field to simulate must be at least twice the length of correlation. Then:

$$\text{length of the field/length of correlation} \geq 2$$

Better results are obtained if this ratio is increased. If this ratio, in practice, is smaller than 2 the length of the field must be increased.

The sampling rate is equal to the point interdistance Δx of the simulation. In practice, the sampling rate must be smaller than the Nyquist rate $(\Delta x)_N$:

$$(\Delta x)_N = \frac{1}{2\Omega}$$

Ω: maximum spectral density.

The spectral density function outside the band $[-\Omega, \Omega]$ is zero or near zero. Usually, Ω is not known as prior information and then we take as sampling rate the point interdistance of the simulation Δx; we could examine the discrete spectral density function calculated in the next step and check that for the highest frequencies the spectral density is near zero, then there is no aliasing (overestimation of a Fourier transform in the highest frequencies) in the discrete Fourier transform. If aliasing is suspected, the sampling rate must be increased (take a smaller Δx), computer the Fourier transform in step 2 and apply the scale theorem of the Fourier transform.

Scale change theorem of the Fourier transform (Weaver, 1989):

$$C(x) \leftrightarrow S(\omega)$$

$$C(ax) \leftrightarrow S(\omega/a)/|a|$$

$a = \Delta x/\Delta x'$, Δx: interdistance between points in the simulation, $\Delta x'$: sampling ratio smaller than Δx (i.e., $a > 1$), $\leftrightarrow$ Fourier transform pair, and $|a|$: absolute value of a. In practice, the most usual case is that it is sufficient to take as sampling ratio the point interdistance of the simulation Δx.

To simulate a nugget effect it is very important to sample the point $\{C(0), x = 0\}$ where all the nugget variance is concentrated.

Step 2: Discrete Spectral Density

Calculation of the spectral density function by the discrete Fourier transform (DFT) of the sampled covariance sequence:

$$S(j) = \frac{1}{N} \sum_{k=0}^{N-1} C(k) \exp(-2\pi kj/N)$$

$\{j = 0, \ldots, N-1\}$. The calculation of the DFT of a sequence made up of N points requires N^2 complex multiplications, which implies an important amount of calculation time. As is well known, the FFT is a numerical algorithm which allows the calculation of the DFT with only $(N \log_2 N)$ operations (Brigham, 1988) which represents an important reduction in calculation time.

As the covariance function has been shifted one must use the shift space theorem (Weaver, 1989) to obtain the correct spectral density function:

$$g(x) = C(x - a)$$

$$C(x) \leftrightarrow S(f)$$

$$g(x) \leftrightarrow G(f)$$

$$C(x - a) \leftrightarrow \exp(-2\pi iaf)S(f)$$

$$S(f) = G(f) \exp(2\pi iaf)$$

x: space coordinate, f: frequency in cycles by interval of data, a: shifted distance, $i = (-1)^{1/2}$: imaginary unity, and $\leftrightarrow$: Fourier transform pair. Steps 1 and 2 are essentially computer calculations of a discrete Fourier transform which define the relation between covariance function and spectral density function. Here is the main strength of the method because any permissible covariance can be sampled including nugget effect, nested structures and anisotropy, and hence can be imposed on the realization that will be obtained in the last step.

In Figs. 3a–c we can see the two-dimensional spectral density functions for the spherical, exponential, and gaussian models of covariance, respectively, calculated in numerical form by means of the fast Fourier transform in two dimensions.

Step 3: Amplitude Spectrum

The discrete amplitude spectrum can be obtained from the discrete spectral density function by the relation seen before:

$$A(j) = \sqrt{S(j)}$$

$\{j = 0, \ldots, N-1\}$, $A(j)$: discrete amplitude, and $S(j)$: discrete spectral density.

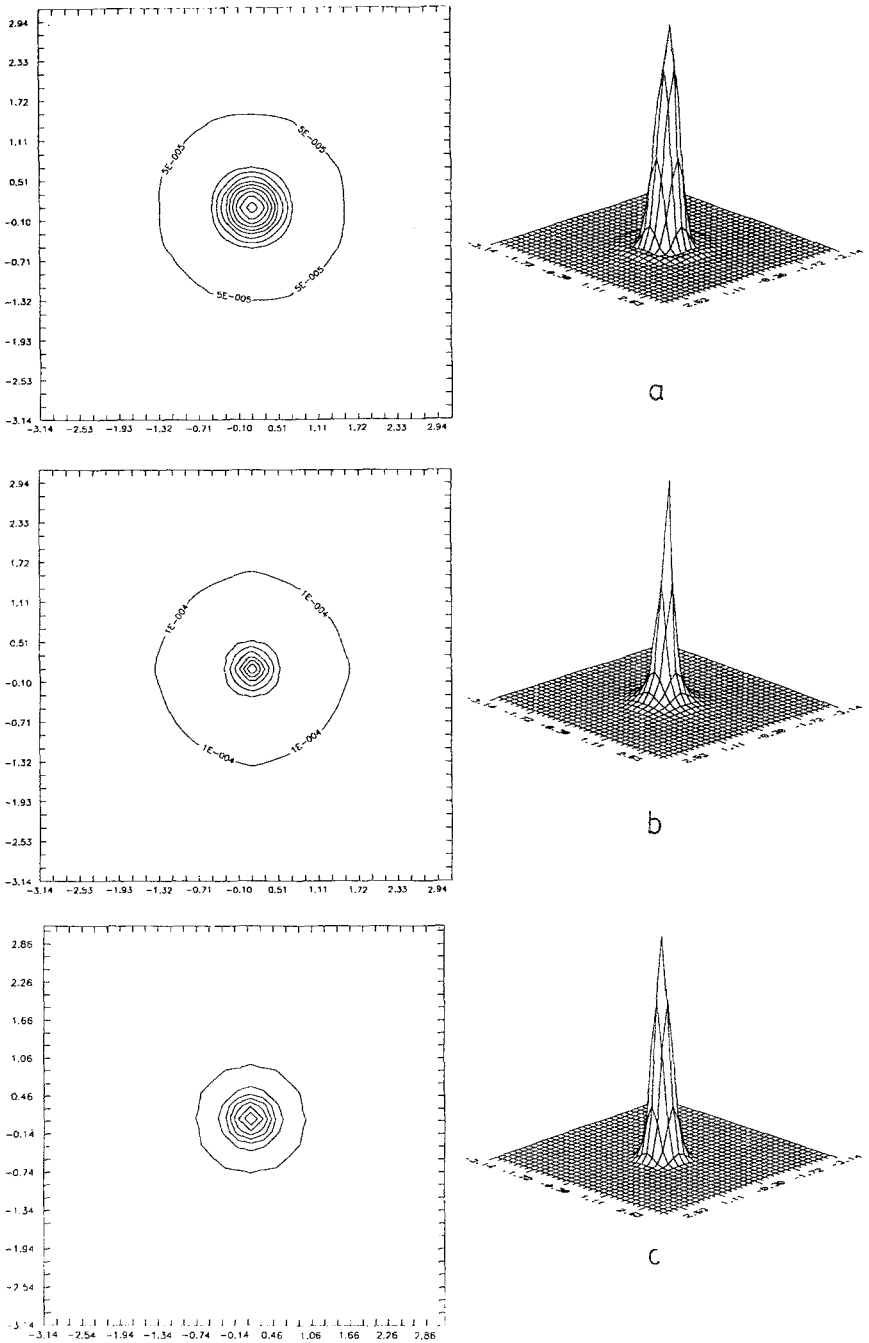

Fig. 3. Two-dimensional spectral density (surface and contour display): (a) spherical model, (b) exponential model, (c) Gaussian model. *X* axis: frequency, *Y* axis: frequency.

Step 4: Phase Spectrum

Generation of a discrete random phase spectrum $\{\varphi(j); j = 0, \ldots, N - 1\}$. $\varphi(j)$ is taken at random from a uniform distribution between 0 and 2π.

$$\varphi(j) = U_j * 2\pi$$

$\{j = 0, \ldots, N - 1\}$, and U_j: random variable uniformly distributed between 0 and 1, generated by any classical subroutine such as that of Schrage (1979).

Step 5: Complex Fourier Coefficients

The Fourier transform of a real function (most usually regionalized variables are real functions) is a hermitian function, i.e., even real part and odd imaginary part (Bracewell, 1986).

As we have seen before the complex coefficients are:

$$A(j) = |A(j)|e^{-i\varphi(j)} = |A(j)| \cos \varphi(j) - i|A(j)| \sin \varphi(j)$$
$$= R(j) - iI(j)$$

$R(j)$ must be even:

$$R(j) = R(-j)$$

$I(j)$ must be odd:

$$I(j) = -I(-j)$$

This can be expressed as symmetries of the coefficients that are specific for 1D, 2D, and 3D. Here index has been expressed with range from 1 to N_1 rather than from 0 to $N_1 - 1$.

In 1D

In following representation, Greek letters represent regions of coefficients:

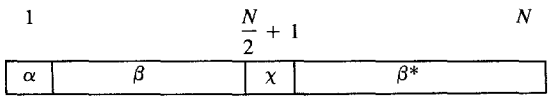

α, χ: real coefficients, β: complex coefficients, and *: complex conjugate. Analytically:

$$A(j) = A^*(N_1 - j + 2) \qquad j \in [2, N_1/2]$$

For example:

$$A(1) = |A(1)| \cos \varphi(1)$$
$$A(2) = |A(2)| \cos \varphi(2) - i|A(2)| \sin \varphi(2)$$
$$A(N_1) = |A(2)| \cos \varphi(2) + i|A(2)| \sin \varphi(2)$$

In this way, we show that the coefficients are hermitian.

In 2D

The symmetries of the complex Fourier coefficients is shown in Fig. 4, it has been verified by direct computation and is similar to those presented by Borgman et al. (1984).

In this figure, the different sectors of Fourier coefficients are represented by different greek letters. The coefficients of sectors of different letters are independent, as are the coefficients of a single sector in themselves. Sectors α, ϑ, ψ, and η are real (the imaginary part is equal to zero) and the rest are complex sectors.

This symmetries can be expressed:

First column

$$A(1, k) = A^*(1, N_2 - k + 2)$$

First row

$$A(j, 1) = A^*(N_1 - j + 2, 1)$$

$(N_1/2) + 1$ column

$$A\left(\frac{N_1}{2} + 1, k\right) = A^*\left(\frac{N_1}{2} + 1, N_2 - k + 2\right)$$

$(N_2/2) + 1$ row

$$A\left(j, \frac{N_2}{2} + 1\right) = A^*\left(N_1 - j + 2, \frac{N_2}{2} + 1\right)$$

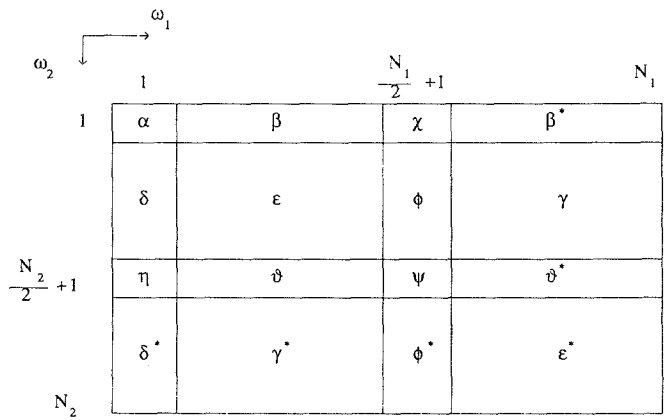

Fig. 4. Complex Fourier coefficients symmetries in 2D. ω: frequency, *: complex conjugate.

Rest of rows and columns

$$A(j, k) = A^*(N_1 - j + 2, N_2 - k + 2)$$

$j \in [2, N_1/2]$, and $k \in [2, N_2/2]$.

In 3D

The arrangement of the discrete complex Fourier coefficients in 3D is shown in Fig. 5. It has been verified by direct computation.

It will be considered that the Fourier coefficients for which the frequency in the third frequency dimension, ω_3, is constant belong to the same level.

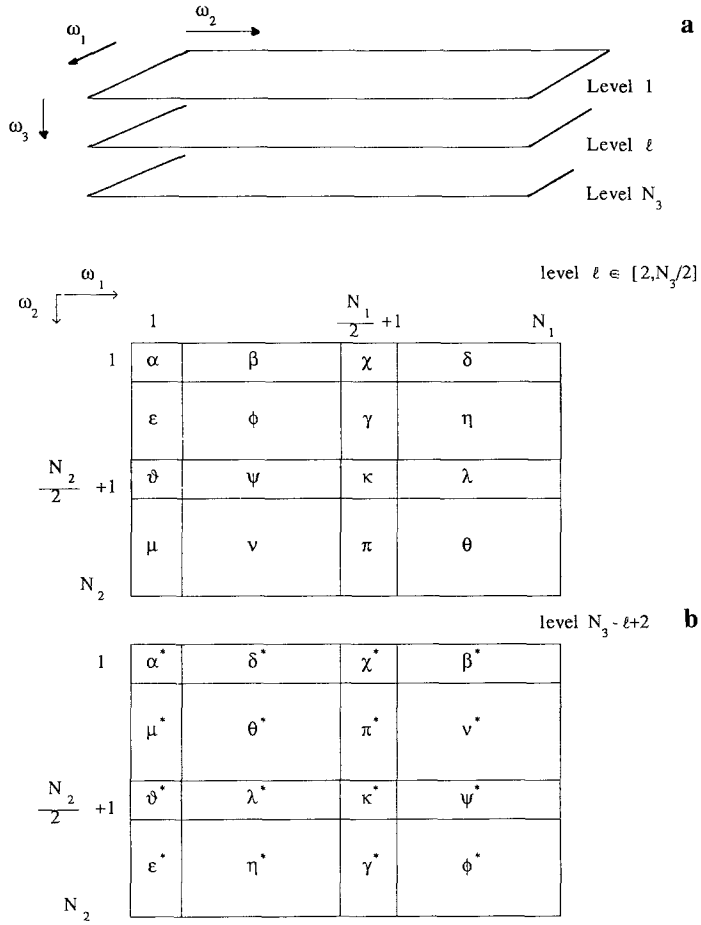

Fig. 5. Arrangement of the complex Fourier coefficients in 3D. (a) Definition of level; (b) Symmetries between the level l and the level $N_3 - l + 2$; $l \in [2, N_3/2]$. *: complex conjugate.

Levels $l = 1$ and $l = (N_3/2) + 1$

At these levels there is an arrangement that is the same as the arrangement of coefficients in 2D shown in Fig. 4:

$$A(1, k, l) = A^*(1, N_2 - k + 2, l)$$

$$A(j, 1, l) = A^*(N_1 - j + 2, 1, l)$$

$$A\left(\frac{N_1}{2} + 1, k, l\right) = A^*\left(\frac{N_1}{2} + 1, N_2 - k + 2, l\right)$$

$$A\left(j, \frac{N_2}{2} + 1, l\right) = A^*\left(N_1 - j + 2, \frac{N_2}{2} + 1, l\right)$$

$$A(j, k, l) = A^*(N_1 - j + 2, N_2 - k + 2, l)$$

$j \in [2, N_1/2]$, and $k \in [2, N_2/2]$.

Rest of the levels

$$l \in [2, N_3/2] \text{ and } l \in \left[\frac{N_3}{2} + 2, N_3\right]$$

The coefficients in level $l \in [2, N_3/2]$ are the complex conjugates of coefficients in level $(N_3 - l + 2)$, according to what is shown in Fig. 5 and that can be expressed analytically:

$$A(1, 1, l) = A^*(1, 1, N_3 - l + 2)$$

$$A\left(1, \frac{N_2}{2} + 1, l\right) = A^*\left(1, \frac{N_2}{2} + 1, N_3 - l + 2\right)$$

$$A\left(\frac{N_1}{2} + 1, 1, l\right) = A^*\left(\frac{N_1}{2} + 1, 1, N_3 - l + 2\right)$$

$$A\left(\frac{N_1}{2} + 1, \frac{N_2}{2} + 1, l\right) = A^*\left(\frac{N_1}{2} + 1, \frac{N_2}{2} + 1, N_3 - l + 2\right)$$

$$A(1, k, l) = A^*(1, N_2 - k + 2, N_3 - l + 2)$$

$$A(1, N_2 - k + 2, l) = A^*(1, k, N_3 - l + 2)$$

$$A(j, 1, l) = A^*(N_1 - j + 2, 1, N_3 - l + 2)$$

$$A\left(\frac{N_1}{2}+1, k, l\right) = A^*\left(\frac{N_1}{2}+1, N_2-k+2, N_3-l+2\right)$$

$$A\left(\frac{N_1}{2}+1, N_2-k+2, l\right) = A^*\left(\frac{N_1}{2}+1, k, N_3-l+2\right)$$

$$A\left(j, \frac{N_2}{2}+1, l\right) = A^*\left(N_1-j+2, \frac{N_2}{2}+1, N_3-l+2\right)$$

$$A\left(N_1-j+2, \frac{N_2}{2}+1, l\right) = A^*\left(j, \frac{N_2}{2}+1, N_3-l+2\right)$$

$$A(j, k, l) = A^*(N_1-j+2, N_2-k+2, N_3-l+2)$$

$$A(N_1-j+2, N_2-k+2, l) = A^*(j, k, N_3-l+2)$$

$j \in [2, N_1/2]$, $k \in [2, N_2/2]$, and $l \in [2, N_3/2]$.

Step 6: Inverse Fourier Transform

Application of the inverse discrete Fourier transform to the complex coefficients $A(j)$ in order to obtain the spatial realization with the covariance function sampled in step 1:

$$z(k) = \sum_{j=0}^{N-1} A(j) \exp(2\pi kj/N)$$

$\{k = 0, \ldots, N-1\}$, and $i = (-1)^{1/2}$. This is done rapidly and efficiently by the fast Fourier transform.

Although in reality there are an infinite number of Fourier coefficients $A(j)$, the method only uses the first N of them. However, as regionalized functions are in general band limited, a sufficiently large value of N gives a reasonable representation of the function. This is the finite discrete approximation to the continuous infinite theory.

CRITERIA OF COMPARISON BETWEEN GENERATORS

1. Ensemble Statistics. These statistics are those which are calculated by taking the average statistics of a high number of realizations. As the number of realizations increases the ensemble statistics tend to become more like their corresponding theoretical values. From a practical point of view we have limited the number of realizations to 100 with the purpose of comparing the results.

The calculated ensemble statistics are: $\bar{x}_m$: mean of 100 realizations, σ_m^2: average variance of 100 realizations, and $\gamma_m(h)$: average variogram of 100 realizations. Likewise, the variance of statistics of each realization with regard to the ensemble statistics is calculated: $\sigma^2(\bar{x})$: variance of the mean of individual

realizations, $\sigma^2(\sigma^2)$: variance of the variance of individual realizations, and $\sigma^2(\gamma(h))$: variance of the variogram of individual realizations. With the purpose of normalizing the variance of the ensemble variogram for the different lags, instead of the last statistic, the coefficient of variation ($C.V.(h)$) will be calculated:

$$C.V.(h) = \frac{\sigma(\gamma(h))}{\gamma_m(h)}$$

A good generator should show good behavior of the ensemble statistics (values close to the theoretical ones) and the dispersion of the statistics corresponding to each realization should be slight with regard to the ensemble value. Really, the results are directly related to the ergodic conditions which depend on the dimensions of the random field and its ratio with the length of correlation.

Conditions of ergodicity are more favorable as

$$\frac{\text{length of the field}}{\text{length of correlation}} \to \infty$$

that can be obtained, for a fixed length of correlation, by increasing the length of the field. But for fixed length of correlation and fixed length of the field, later ensemble statistics can be used for comparison of results of different generators.

2. *Statistics of a Single Realization.* The following statistics are considered for a single realization taken at random: $\bar{x}$: mean, σ^2: variance, and $\gamma(h)$: variogram. For fixed conditions of ergodicity, it is expected that the fit between experimental statistics of a realization taken at random and theoretical statistics are close as the ensemble statistics show a good behavior (in the sense indicated before).

3. *Behavior of the Variogram over Great Distances.* It is necessary to ensure that the variogram function of the simulation does not show periodicities, which is checked by calculating that function over long distances. (This feature has its main interest in 1D long series.)

RESULTS

In 1D, the one-dimensional variogram models for which the methodology has been checked are as follows:

Spherical model

$$\gamma(h) = \begin{cases} \sigma^2 \left[\dfrac{3h}{2a} - \dfrac{1}{2} \left(\dfrac{h}{a} \right)^3 \right] & h \in [0, a] \\ \sigma^2 & h \geq a \end{cases}$$

Exponential model

$$\gamma(h) = \sigma^2[1 - \exp(-h/a)]$$

Gaussian model

$$\gamma(h) = \sigma^2[1 - \exp(-h^2/a^2)]$$

Triangular model

$$\gamma(h) = \begin{cases} \sigma^2(h/a) & h \in [0, a] \\ \sigma^2 & h \geq a \end{cases}$$

Hole I model

$$\gamma(h) = \sigma^2\left(1 - \left[\left(1 - \frac{h}{a}\right)\exp(-h/a)\right]\right)$$

Hole II model

$$\gamma(h) = \sigma^2(1 - \exp(-h/a)\cos(hb))$$

where $\gamma(h)$: variogram function, h: lag of variogram, a: range or length of correlation, σ^2: sill or variance, and b: cosine function constant. In this paper, only the complete results for the spherical variogram (or covariance) model will be presented, comparing the results of the spectral method herein developed with the classical method of Shinozuka and Jan (1972); the conclusions are valid for the rest of the models. A more detailed discussion of the results can be found in Pardo-Igúzquiza (1991). The theoretical mean and variance are valued zero and one respectively.

Shinozuka and Jan (1972) Method in 1D

To compare this method and FIM each realization is a sequence of 1000 points equally spaced, with interpoint distance Δx equal to one. The spectral density function that corresponds to a one-dimensional spherical covariance function is (Pardo-Igúzquiza, 1991):

$$S(\omega) = \frac{3\sigma^2}{2\pi\omega^3 a^2}\left(\sin(\omega a) + \frac{1}{\omega a}(\cos(\omega a) - 1)\right)$$

σ^2: variance, and a: range. This function is near zero outside the maximum spectral frequency $\Omega = 32/a$. The number of harmonics M has been stated to 100, because good results are reported by Shinozuka and Jan (1972), Mantoglou and Wilson (1982) and ourselves for this number of harmonics.

The model of covariance to impose is a spherical model with range 10 units and a unity sill:

$$C(h) = \mathrm{Sph}(1.)_{10}$$

Sph $(a)_b$: Spherical model with range b and sill a. The results are shown in Table I and in Fig. 6a–d. Good behavior of the ensemble statistics can be seen along with a very small dispersion of the statistics of each realization with regard to the ensemble value. The ensemble variance is always slightly lower than the theoretical value since the generator integrates the spectral density function for a limited frequency band. The main inconvenience of the method is that the variogram of the simulation is periodic as indicated before, with period $T = 4\pi M/\Omega$, and as indicated by Black and Freyberg (1990), only a part of the realization would be usable. However, the period can be increased if the number of harmonics is increased with the corresponding increase in calculus time.

FIM in 1D

Each realization has 1000 points (on a simulate $2^{10} = 1024$ points and on taking the first 1000 points) with interdistance unity; the model of covariance is the same as imposed in the previous method.

The results for this method can be found in Table II and Fig. 7a–d. The good behavior of the ensemble statistics is noticeable, the dispersion of the statistics for each realization with regard to the ensemble value is slight and, in addition, the variogram of the simulation shows no kind of periodic behavior. Theoretically the variogram is periodic with period equal to the length of the field N (theorem of the periodicity of the discrete Fourier transform; Weaver, 1989):

$$\gamma(k) = \gamma(k + N)$$

$k = 1, 2, 3, \ldots N$. Then the periodicity cannot be detected in the realization and all the length of the series is usable.

Table I. Average Statistics of 100 Realizations[a]

Variogram Model	$\bar{x}$	$\sigma^2(\bar{x})$	σ^2	$\sigma^2(\sigma^2)$
Spherical	−.0031	.0012	.9674	.0001
Triangular	.0038	.0012	.9701	.0010
Exponential	−.0014	.0006	.9708	.0001
Gaussian	.0016	.0084	.9869	.0010
Hole I	.0001	.0000	.9679	.0000
Hole II	−.0003	.0000	.9844	.0000

[a] Shinozuka and Jan (1972) method. $\bar{x}$: mean, $\sigma^2(\bar{x})$: variance of the mean, σ^2: variance, $\sigma^2(\sigma^2)$: variance of the variance.

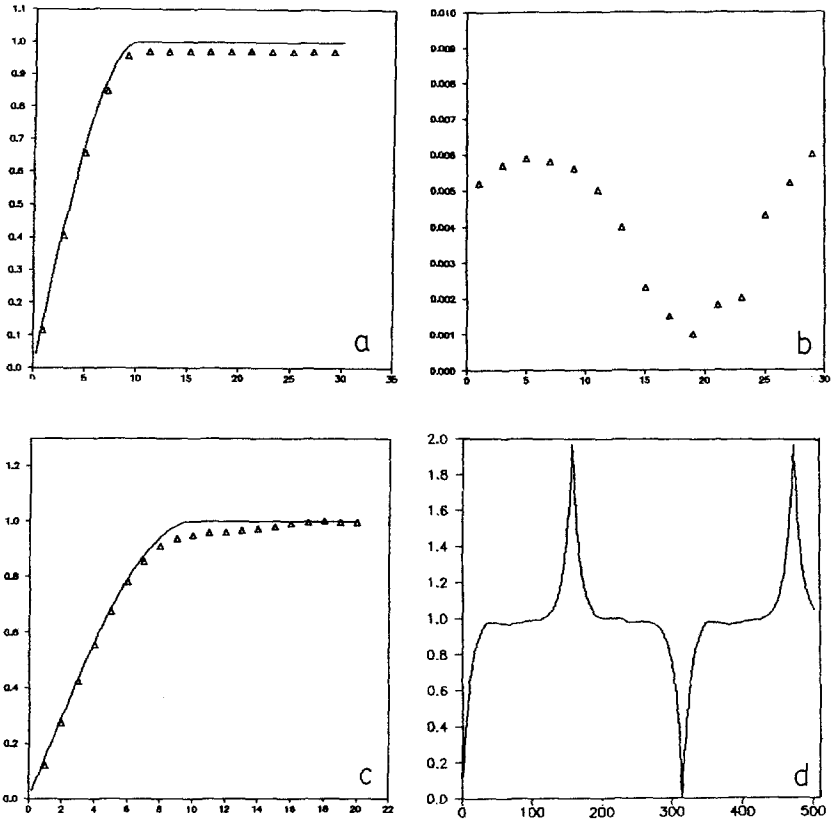

Fig. 6. Results of the Shinozuka and Jan (1972) method in 1D. (a) average variogram for 100 simulations. Δ: simulation, ——: model. (b) Coefficient of variation of average variogram. Δ: simulation. (c) Variogram of a single realization. Δ: simulation, ——: model. (d) Variogram of a single realization over great distances. ——: simulation, X axis: distance, Y axis: variogram (a, c, and d), and coefficient of variation (b).

Table II. Average Statistics of 100 Simulations[a]

Variogram Model	$\bar{x}$	$\sigma^2(\bar{x})$	σ^2	$\sigma^2(\sigma^2)$
Spherical	.0102	.0034	.9931	.0001
Triangular	.0059	.0047	.9914	.0002
Exponential	−.0014	.0040	.9901	.0002
Gaussian	−.0049	.0054	.9873	.0003
Hole I	−.0027	.0001	.9987	.0000
Hole II	−.0034	.0008	.9985	.0001

[a] Fourier integral method. $\bar{x}$: mean, $\sigma^2(\bar{x})$: variance of the mean, σ^2: variance, $\sigma^2(\sigma^2)$: variance of the variance.

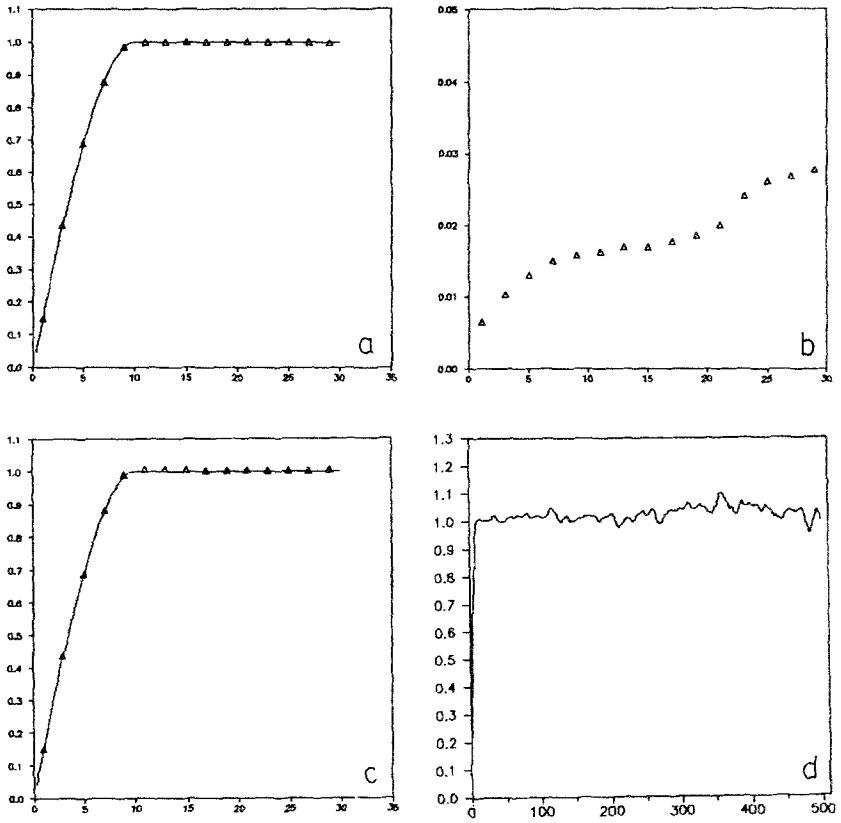

Fig. 7. Results of the FIM in 1D. (a) Average variogram for 100 simulations. Δ: simulation, ——: model. (b) Coefficient of variation of average variogram. Δ: simulation. (c) Variogram of a single realization. Δ: simulation, ——: model. (d)Variogram of a single realization over great distances. ——: simulation, *X* axis: distance, *Y* axis: variogram (a, c, and d), and coefficient of variation (b).

DISCUSSION

The main inconvenience of the Shinozuka and Jan (1972) method is the periodicity of the simulated variogram (as was indicated by Black and Freyberg, 1990), the period of which is smaller than the period of the variogram simulated by the FIM.

The basis of the Fourier integral method is the same as used by Fox (1987) to generate realizations in 1D imposing the fractal dimension of the process. The particularities that are presented in this paper have been the adaptation in order to simulate any covariance model, since the spectral density function is calculated by FFT from an adequate sampling of the covariance function. This

allows the integration in a single process of the simulation of nested structures, one of which could be a nugget effect (examples in 2D will be shown).

The simulation variogram does not show periodicity (in the sense indicated before, the period is really too long to be detected). The coefficient of variation of the different realizations is kept within acceptable limits. This, together with the good behavior of the ensemble statistics means that, on taking a single realization at random, its variogram is expected to be acceptable (a good fit between experimental and theoretical values). The time of calculus consumed for generating a series of 1000 points long is shown in Table VII. The Shinozuka and Jand method requires, for this example, three times more time.

TBM in 2D

The TBM has been used with 16 lines (Mantoglou and Wilson, 1982) and the width of the bands is equal to one half of the spacing between the points of the simulation network. Similar results have been obtained using different one-dimensional generators on the lines. Here one presents results with the FIM as a one-dimensional generator. Each realization consists of 4096 values arranged in a regular network of 64 × 64 points with separation of one on X and Y axes (Δx and Δy). The imposed covariance is:

$$C(h) = \mathrm{Sph}(1.)_{10}$$

The one-dimensional covariance function to be simulated on the lines can be found in Brooker (1985). Figures 8a–d show the average variogram of 100 realizations for directions N-S, E-W, NE-SW, and NW-SE. The experimental values and the corresponding theoretical ones are quite similar. Figure 8e shows the coefficient of variation $C.V.(h)$ of the average variogram, as can be seen in the above figure, the statistics show similar behavior in all directions and the same value of around 0.14 (14%). Last, Fig. 8f represents the experimental variogram of a single realization. In Table III, the statistics of the different realizations are registered.

TBM in 3D

The TBM is used with 15 lines which join the middle points of the edges of an icosahedron (Journel, 1974). A one-dimensional process is generated on each line by means of the FIM as spectral generator. In each realization, a total of 4096 points has been simulated in a regular network of 16 × 16 × 16 on X, Y, and Z axes. The distance between the points is one ($\Delta x = \Delta y = \Delta z = 1$) and the simulated model is:

$$C(h) = \mathrm{Sph}(1)_5$$

The average variogram of 100 realizations for the directions X, Y, and Z re-

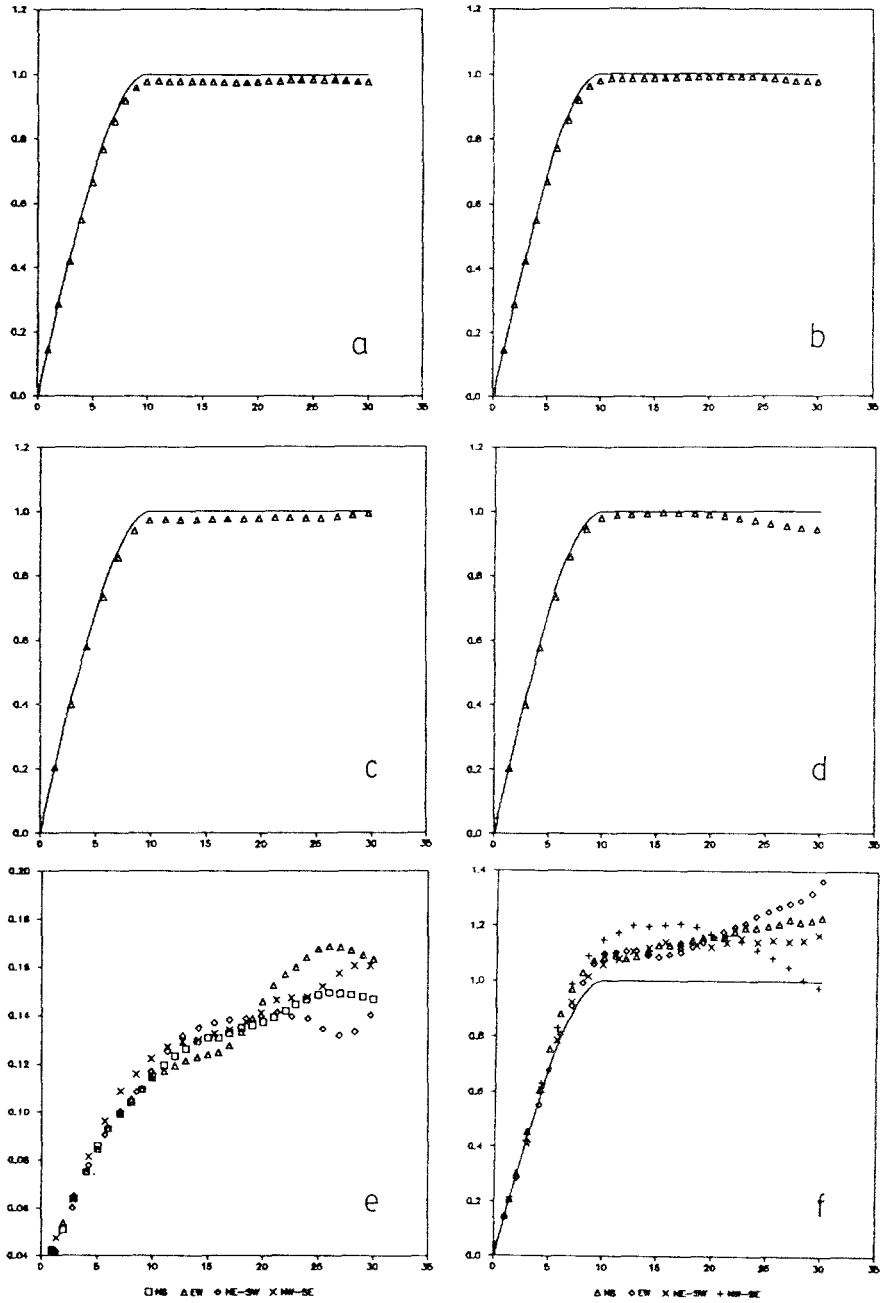

Fig. 8. Results of the TBM in 2D with isotropic covariance. Average variogram of 100 realizations for directions: (a) N-S, (b) E-W, (c) NE-SW, (d) NW-SE, (e) coefficient of variation, (f) directional variograms of a single realization. X axis: distance, Y axis: variogram function (a, b, c, d, and f), and coefficient of variation (e). ——: model, Δ, o, $+$, x: simulation.

Table III. Statistics of the Simulation[a]

	$\bar{x}$	$\sigma^2(\bar{x})$	σ^2	$\sigma^2(\sigma^2)$
Theoretical	.0	.0	1.0	.0
100 Realizations	.0114	.0152	.9780	.0097
One realization	.1059	—	1.1662	—

[a]TBM in 2D. $\bar{x}$: mean, $\sigma^2(\bar{x})$: variance of the mean, $\sigma^2(\sigma^2)$: variance of the variance.

spectively is presented in Fig. 9a–c. We can see that the results are close to the corresponding theoretical values. Figure 8d shows the coefficient of variation of the average variogram for 100 realizations, given an order of magnitude around 0.15 (15%) which is similar to that obtained with the TBM in 2D.

Figure 9e shows the simulated variogram of a realization chosen at random, where divergences can be observed between experimental and theoretical values of the simulation. Table IV gives the statistics of the different simulations.

FIM in 2D

Figures 10a–d shows the average variogram of 100 realizations in accordance with the directions N-S, E-W, NE-SW, and NW-SE, respectively. Experimental and theoretical values fit well. Each realization consists of 4096 points arranged in a regular network of 64 × 64 points with point interdistance $\Delta x = \Delta y = 1$. The imposed covariance function is:

$$C(h) = \mathrm{Sph}(1.)_{10}$$

Figure 10e shows the estimated experimental variogram of a single realization. Slight fluctuations can be observed but the similarity with regard to the theoretical model can be considered acceptable. The cartography of this realization is shown in Fig. 11. Table V gives the statistics of the previous realizations. As has been noticed before, the simulation of a nugget effect and nested structures does not require any additional calculus or computing time, because this feature is integrated in step 1 of the FIM where the covariance function model to be simulated is sampled.

Figures 12a–b show the estimated experimental variograms of a single random realization (64 × 64 = 4096 points; $\Delta x = \Delta y = 1$) where the covariance function has a nugget effect of 50% of the total variance:

$$C(h) = 0.5 + \mathrm{Sph}(0.5)_{20.}$$

The great similarity between experimental and theoretical values is noticeable. Figure 13 shows the cartography of this realization. In order to show the simulation of nested structures a realization of 4096 points (64 × 64) and unit

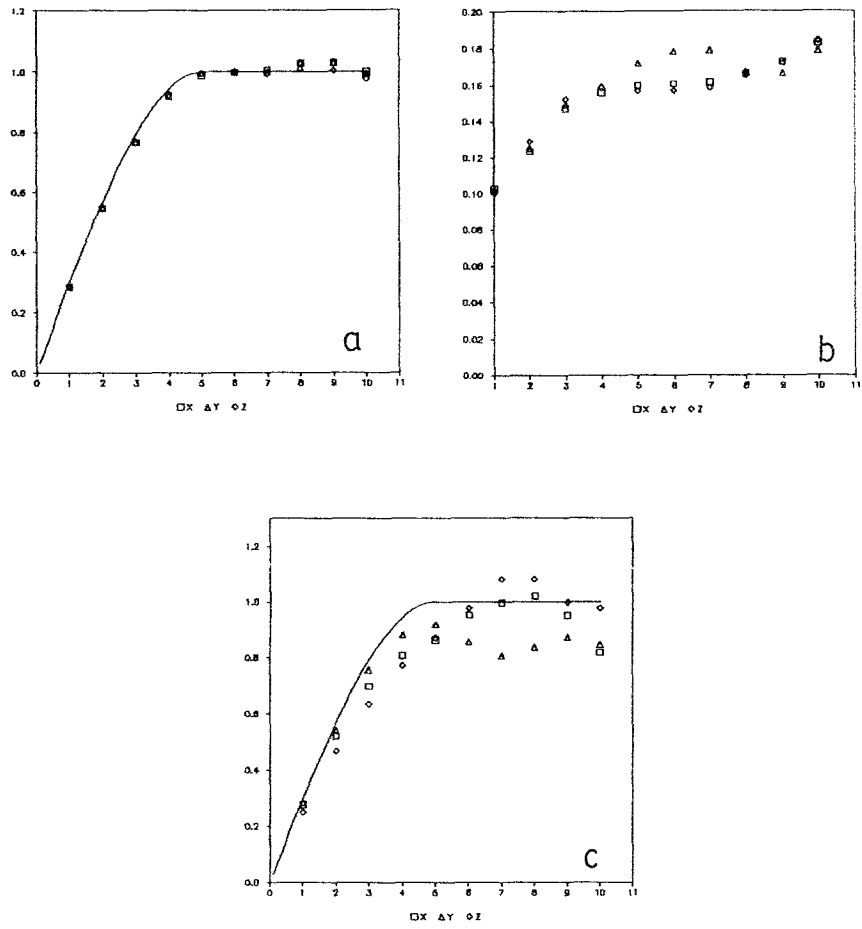

Fig. 9. Results of the TBM in 3D with isotropic covariance. (a) Average variograms of 100 realizations for X, Y, and Z directions. (b) Coefficient of variation. (c) Experimental variogram of a single random realization. X axis: distance, Y axis: variogram function (a, c), and coefficient of variation (b). ——: model, □, Δ, o: simulation.

Table IV. Statistics of the Simulation[a]

	$\bar{x}$	$\sigma^2(\bar{x})$	σ^2	$\sigma^2(\sigma^2)$
Theoretical	.0	.0	1.0	.0
100 Realizations	−.0043	.0124	.9716	−.0166
One realization	−.1570	—	1.0365	—

[a]TBM in 3D. $\bar{x}$: mean, $\sigma^2(\bar{x})$: variance of the mean, σ^2: variance, $\sigma^2(\sigma^2)$: variance of the variance.

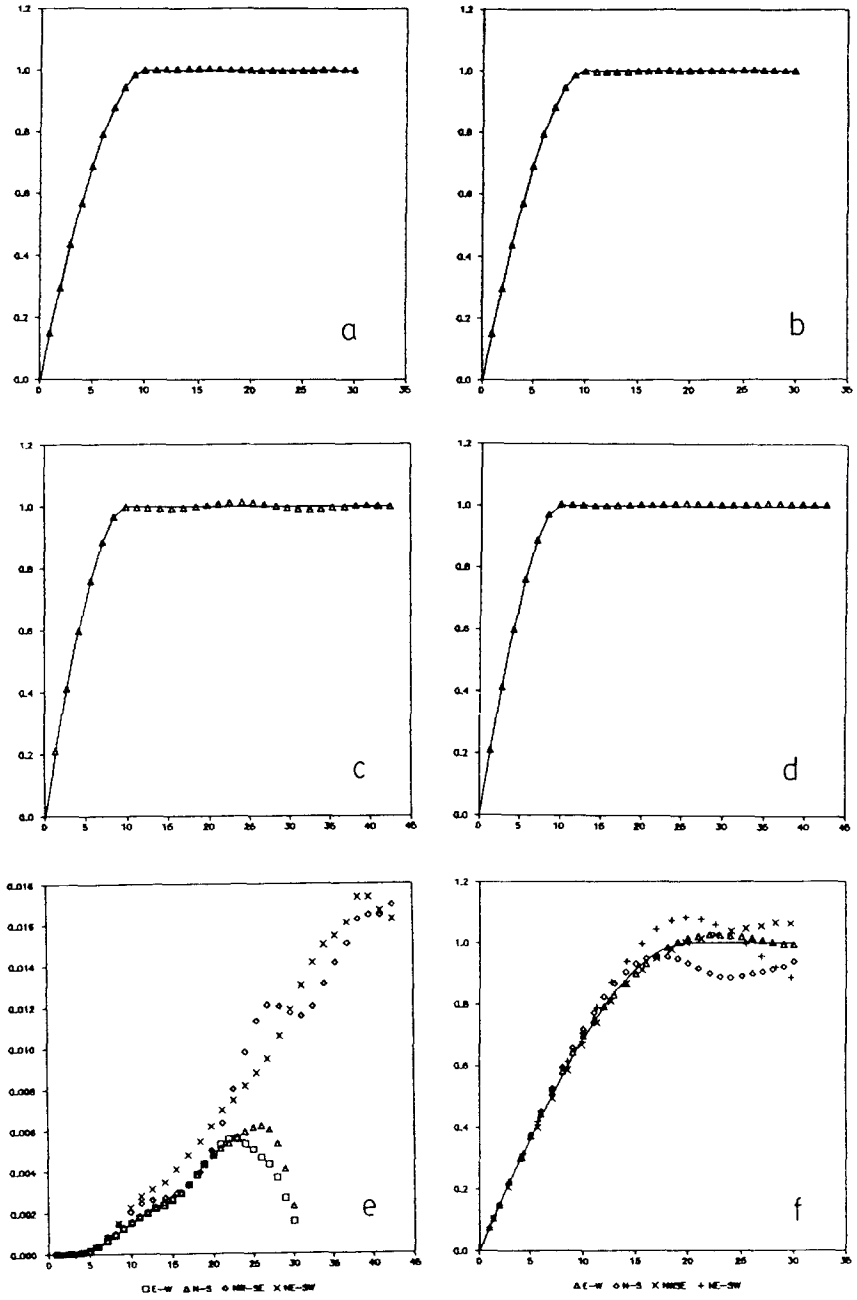

Fig. 10. Results of the FIM in 2D with isotropic covariance. Average variogram of 100 realizations for directions: (a) N-S, (b) E-W, (c) NE-SW, (d) NW-SE, (e) coefficient of variation, (f) variogram of a single realization. X axis: distance, Y axis: variogram function (a, b, c, d, and f), and coefficient of variation (e). ——: model, Δ, o, $+$, x: simulation.

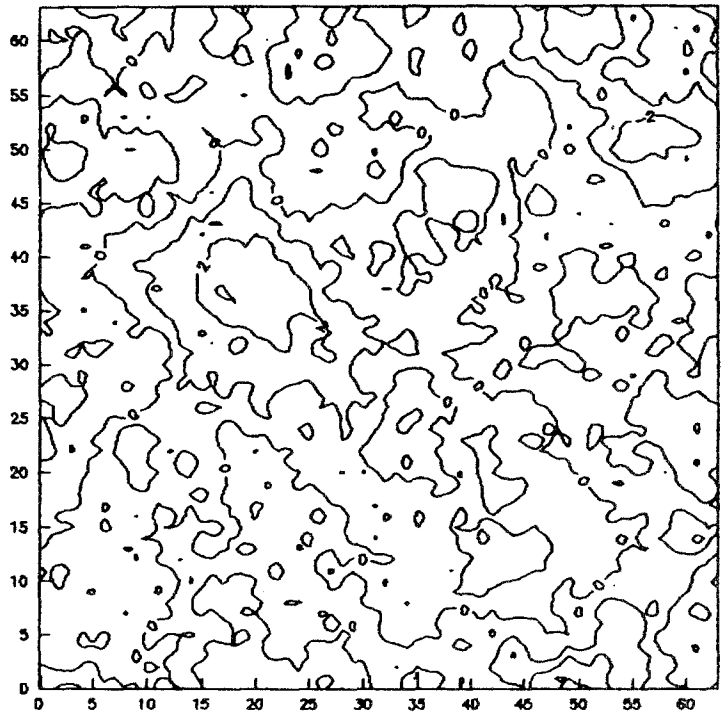

Fig. 11. Cartography of a single isotropic realization. X axis: distance, Y axis: distance.

Table V. Statistics of the Simulation[a]

	$\bar{x}$	$\sigma^2(\bar{x})$	σ^2	$\sigma^2(\sigma^2)$
Theoretical	.0	.0	1.0	.0
100 Realizations	.0047	.0079	.9846	−.0000
One realization	−.1030	—	.9693	—

[a] FIM in 2D. $\bar{x}$: mean, $\sigma^2(\bar{x}$: variance of the mean, σ^2: variance, $\sigma^2(\sigma^2)$: variance of the variance.

interdistance ($\Delta x = \Delta y = 1$) is simulated, imposing a model of covariance with three spherical nested structures:

$$C(h) = \text{Sph}(0.3)_{10} + \text{Sph}(0.3)_{15} + \text{Sph}(0.4)_{20}$$

Figures 14a–f show the result; a good fit between experimental and theoretical values can be seen.

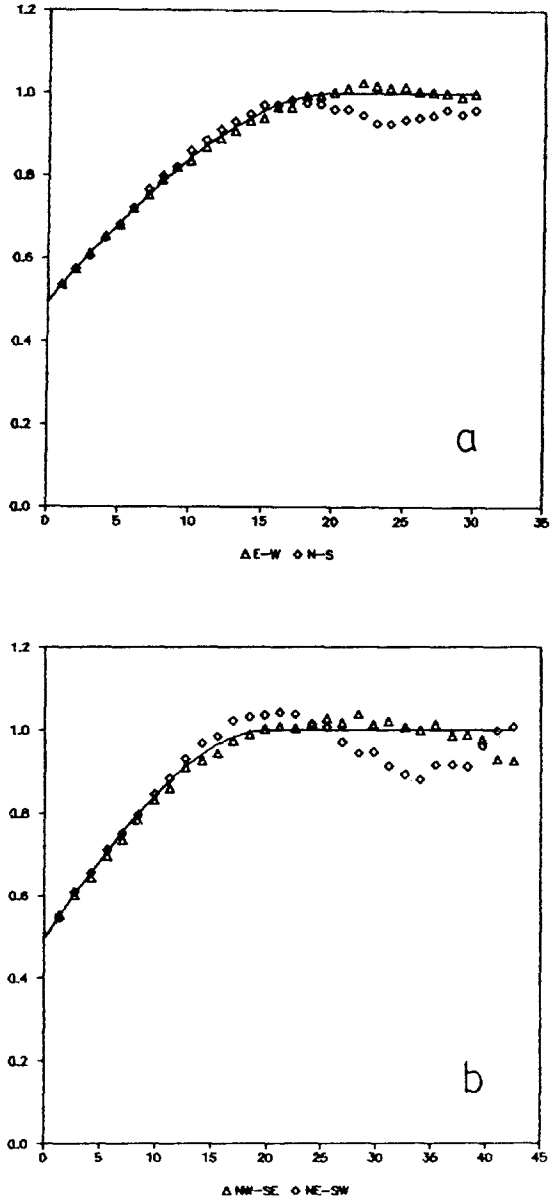

Fig. 12. Results of the FIM in 2D. Experimental variograms of a single random realization with nugget effect. (a) N-S and E-W directions. (b) NE-SW and NW-SE directions. X axis: distance, Y axis: variogram function. ——: model, Δ, o: simulation.

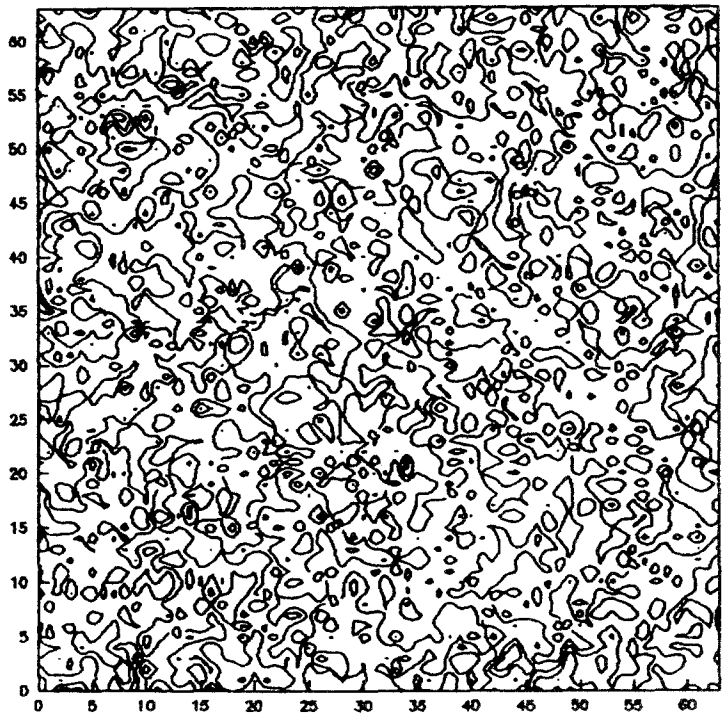

Fig. 13. Cartography of a single realization with nugget effect which represents 50% of the total variance. X axis: distance, Y axis: distance.

FIM in 3D

A three-dimensional network is simulated consisting of 4096 points ($16 \times 16 \times 16$) imposing a spherical covariance model with parameters:

$$C(h) = \mathrm{Sph}(1.)_5$$

The theoretical and experimental statistics of one realization, along with the average values of 100 realizations are shown in Table VI.

Figure 15a shows the average variogram of 100 realizations on the three axes of coordinates, and it can be seen how the connection between the variogram model and the average variogram of the simulation is perfect. The simulated variogram in a single random realization in the directions X, Y, and Z is shown in Fig. 15b, showing a strong similarity between experimental and theoretical values. The coefficient of variation for the variogram function of the 100 realizations is shown in Fig. 15c and is approximately 0.002 (0.2%). Table VI gives the statistics of the previous realizations.

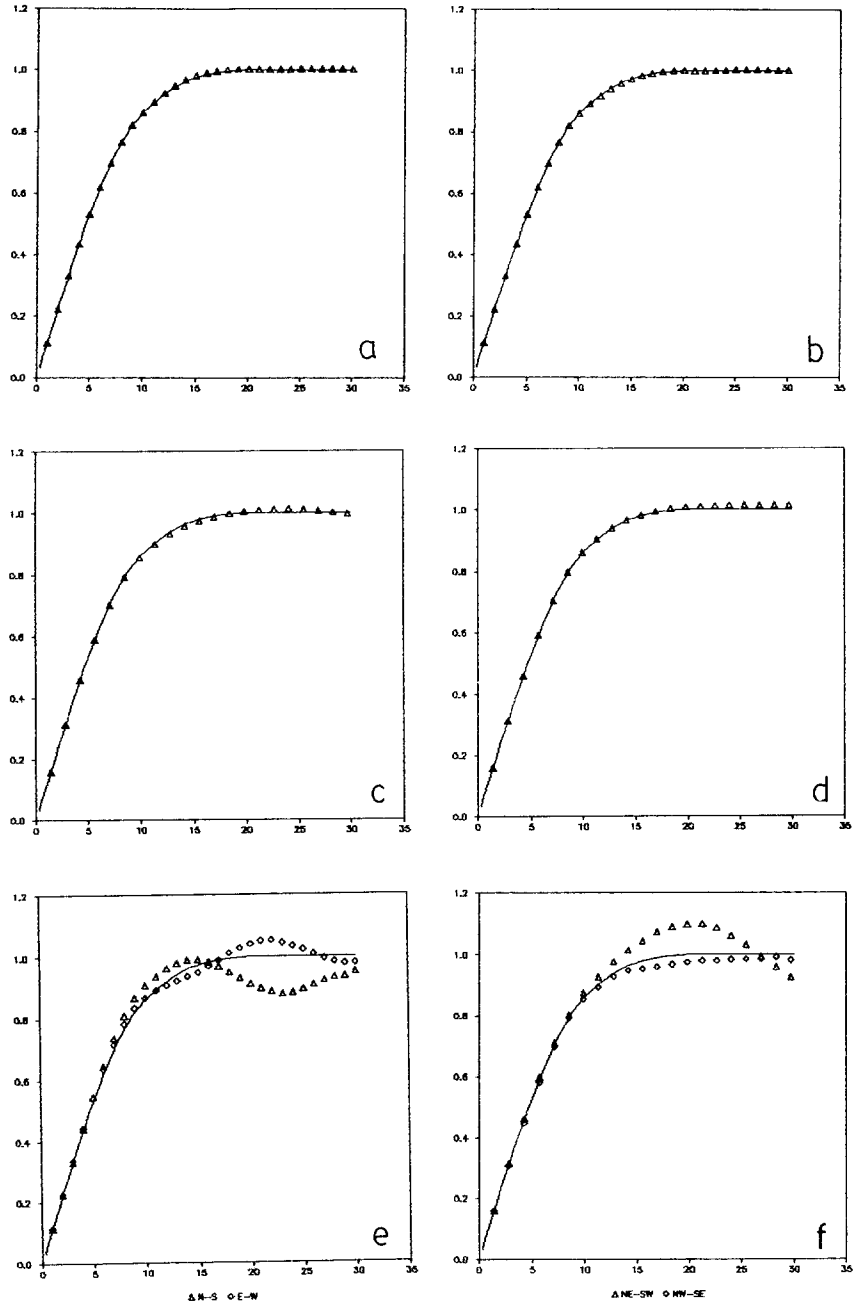

Fig. 14. Results of the FIM in 2D. Realizations with a covariance model with three nested structures. Average variogram of 100 realizations for directions: (a) N-S, (b) E-W, (c) NE-SW, (d) NW-Se. Variograms of a single realization for directions: (e) N-S and E-W, (f) NE-SW and NW-SE. X axis: distance, Y axis: variogram function. ——: model, Δ, o: simulation.

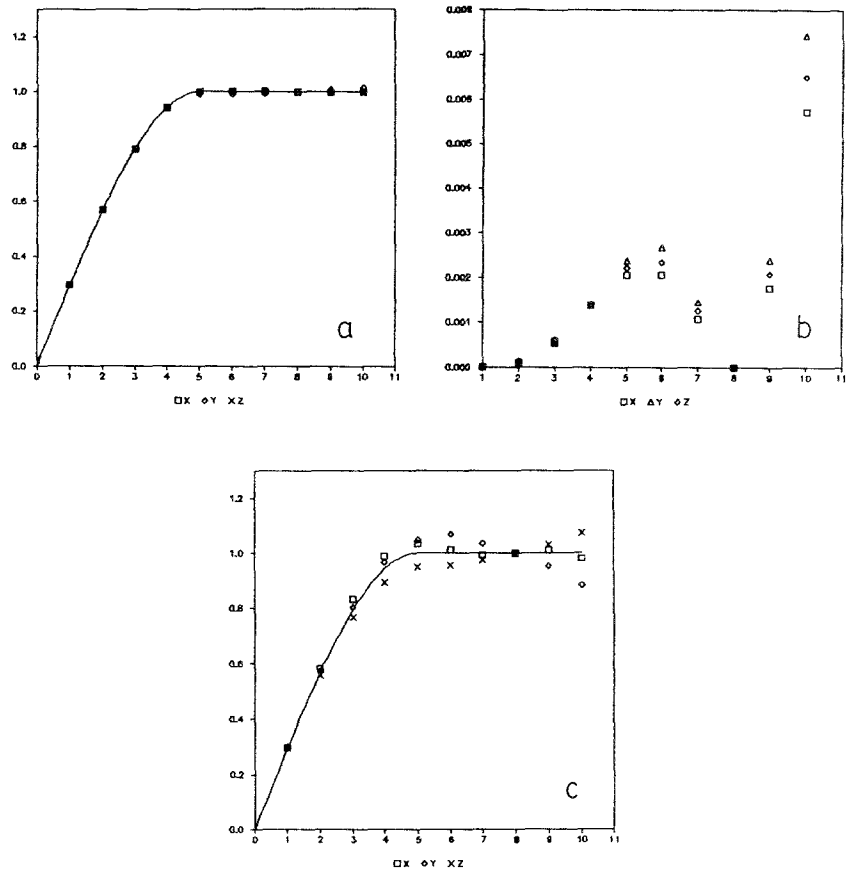

Fig. 15. Results of the FIM in 3D with isotropic covariance: (a) average variograms of 100 simulations for X, Y, and Z directions, (b) coefficient of variation, (c) experimental variograms of a single random realization. X axis: distance, Y axis: variogram function (a, b) and coefficient of variation (b). ——: model, □, Δ, o: simulation.

Table VI. Statistics of the Simulation[a]

	$\bar{x}$	$\sigma^2(\bar{x})$	σ^2	$\sigma^2(\sigma^2)$
Theoretical	.0	.0	1.0	.0
100 Realizations	.0028	.0084	.9830	−.0000
One realization	−.0744	—	.9832	—

[a] FIM in 3D. $\underline{x}$: mean, $\sigma^2(\underline{x})$: variance of the mean, σ^2: variance, $\sigma^2(\sigma^2)$: variance of the variance.

DISCUSSION

In practice, either of the two methods studied previously, TBM or FIM, can be chosen. Each of these methodologies has its advantages and disadvantages which are considered below. The complexity and programming of the two methods are quite similar. Both techniques are relatively simple from a conceptual point of view and are easy to program. However, in practice, the spectral method described has the advantage of allowing us to consider any type of covariance function however complicated its analytical expression may be. On the contrary, to apply the TBM it is necessary to know the one-dimensional covariance function or the spectral density function, which are to be used in the generating process. The precision of both techniques, considering the ensemble statistics and variogram, shows a good fit between experimental and theoretical values. However, there is a serious divergence between both methods when considering the dispersion of the variogram of each realization with regard to the ensemble variogram. This dispersion is represented by the coefficient of variation of the average variogram.

The FIM presents a coefficient of variation of 0.01 (1%) clearly lower than the coefficient of variation obtained by TBM, 0.15 (15%). This relatively noticeable difference in the coefficient of variation has importance when a single random realization is considered; the divergences between experimental and theoretical values are less for the FIM than for the TBM. The time required to generate one realization of the examples previously presented on a PC-386 compatible is shown in Table VIII. The FIM method only requires, for the examples presented, 20% more time than the TBM, which in practice is a few seconds more. The disadvantages of the FIM is that it uses a regular network for simulation and the number of points on the X, Y, and Z axes has to be a multiple of two. With the TBM any number of points in any location can be simulated.

In Pardo-Igúzquiza (1991), a practical method is presented for the simu-

Table VII. Time Consumption by the Different Methods in the Different Examples

Dimensions	Points	Generator	CPU time (seconds and hundredth of a second)
1 D	1000	Shinozuka and Jan	15.44
		FIM	4.40
2 D	4096	TBM	7.68
		FIM	8.95
3 D	4096	TBM	6.81
		FIM	9.01

lation of values in any location from the simulated values in a regular grid. On the other hand, to solve the second problem, it is enough to simulate a realization of greater size and then take the area of interest. In the same way as occurs with the TBM, the realizations generated by the FIM has a multivariate gaussian distribution. Therefore each realization is gaussian and, moreover, on taking into account a large number of realizations, each random variable (different values at the same location) is likewise gaussian. One hundred realizations have been simulated on a grid of 64 × 64 values. One location has been selected at random from the 4096 possible locations. Figure 16 shows the histogram and the statistics for the 100 values of the random function in the same location previously chosen. It can be seen how the histogram comes close to representing a gaussion distribution with zero mean and unity variance. Therefore, there is variation from one realization to another of the same random function and the realizations generated by the FIM can be used in sensitivity studies. This feature (realizations simulated must not be restricted to an artificially narrow range of variation) must be checked for any simulation methodology (Dowd, 1991).

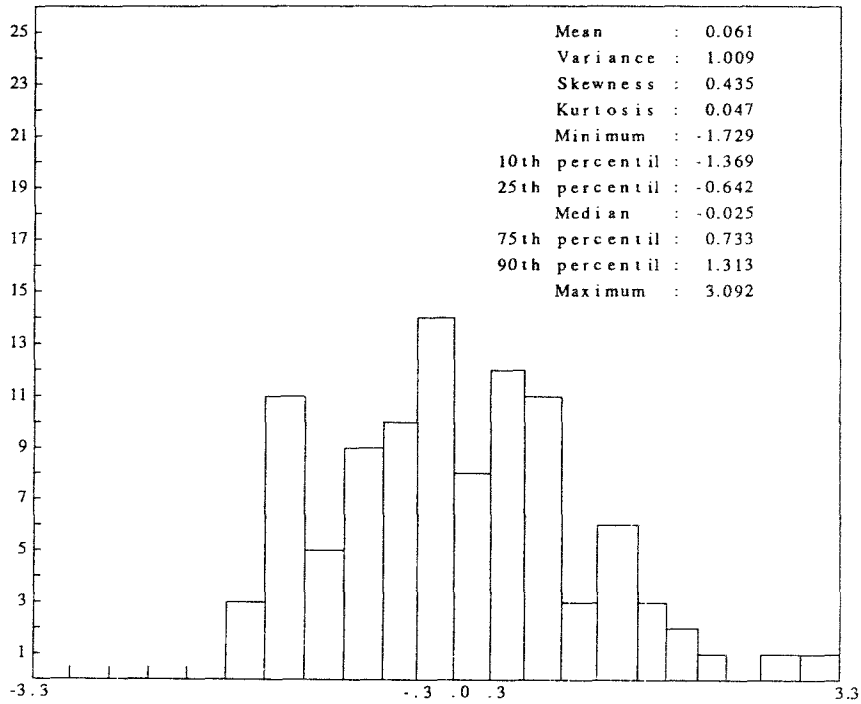

Fig. 16. Histogram and statistics of 100 values of a random variable generated in 100 different realizations by the FIM in the same grid point previously chosen at random. *X* axis: gaussian value, *Y* axis: absolute frequency.

Simulations of Realizations with Anisotropic Covariance by the FIM

A random field which represents a regionalized variable is said to be anisotropic when the variability is not the same in all directions. That is to say, the covariance function (or the variogram) depends on the direction.

Geometric Anisotropy

A variogram has a geometric anisotropy when the variogram has the same sill in all directions but the range depends on the direction (Isaaks and Srisvastava, 1991). For the generation of realizations of a random function with geometric anisotropic covariance there are different working alternatives, such as that proposed by Journel and Huijbregts (1978) based on a cartesian coordinates transform or that proposed by Mantoglou (1987) using the TBM with a one-dimensional spectral generator.

It is also possible to simulate anisotropic random fields by the FIM. The basis is as simple as sampling the anisotropic covariance function and calculating the corresponding spectral density function (Fig. 17a). The remaining steps are the same as those described previously. To check this, 100 realizations of 4096 (64×64) points each has been generated. The covariance function imposed is a spherical model that presents a geometric anisotropy with a range of 20 units in the N-S direction and 10 units in the E-W direction:

$$C(x, y) = \left[1 - \frac{3}{2}\frac{x}{a_x} + \frac{1}{2}\frac{x^3}{a_x^3}\right] + \left[1 - \frac{3}{2}\frac{y}{a_y} + \frac{1}{2}\frac{y^3}{a_y^3}\right]$$

$a_x = 10$: range in the N-S direction (X axis), $a = 20$: range in the E-W direction (Y axis), and sill $= 1$.

The point interdistance in the X and Y axes are equal to one ($\Delta x = \Delta y = 1$). Figures 18a–d show the average variogram obtained from 100 independent realizations for the direction N-S, E-W, NW-SE, and NE-SW, respectively. The good correlation between the theoretical and the experimental values can be observed. Figures 18e–f show the experimental variogram for a single random realization and, last, Fig. 19 shows the cartography of isovalues for this realization.

Zonal Anisotropy

A covariance model has a zonal anisotropy when the range is the same in all directions but the sill varies with the direction (Isaaks and Srisvastava, 1989). To check the simulation of a zonal anisotropy in two dimensions, 100 realizations of 4096 (64×64) points have been generated. The covariance function imposed is:

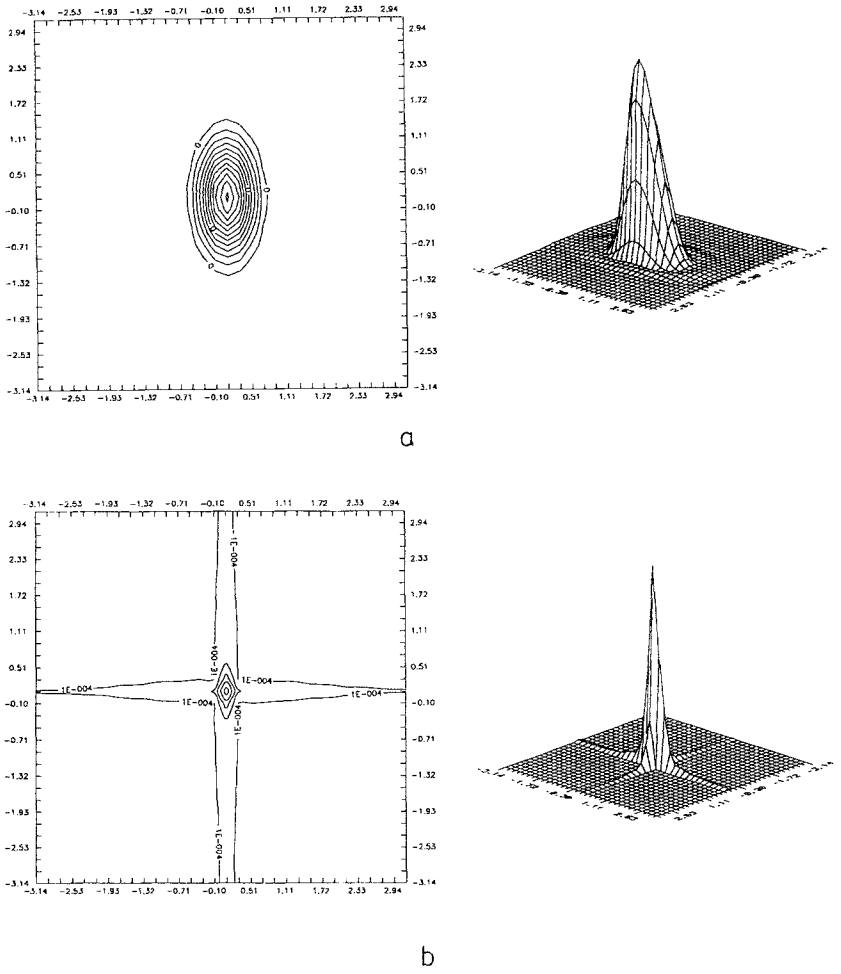

Fig. 17. Two-dimensional anisotropic spectral density function (surface and contour display): (a) geometric anisotropy, (b) zonal anisotropy. X axis: frequency, Y axis: frequency.

$$C(x, y) = C_x\left[1 - \frac{3}{2}\frac{x}{a} + \frac{1}{2}\frac{x^3}{a^3}\right] + C_y\left[1 - \frac{3}{2}\frac{y}{a} + \frac{1}{2}\frac{y^3}{a^3}\right]$$

$a = 10$: isotropic range, $C_x = 0.3$: sill in the X direction, and $C_y = 0.7$: sill in the Y direction. Figure 17b shows the spectral density function of a covariance with zonal anisotropy. Figure 20 shows the results of the simulation, and in Fig. 21 the cartography of a single realization has been represented. In practice, zonal anisotropy and geometric anisotropy can occur together on the same ran-

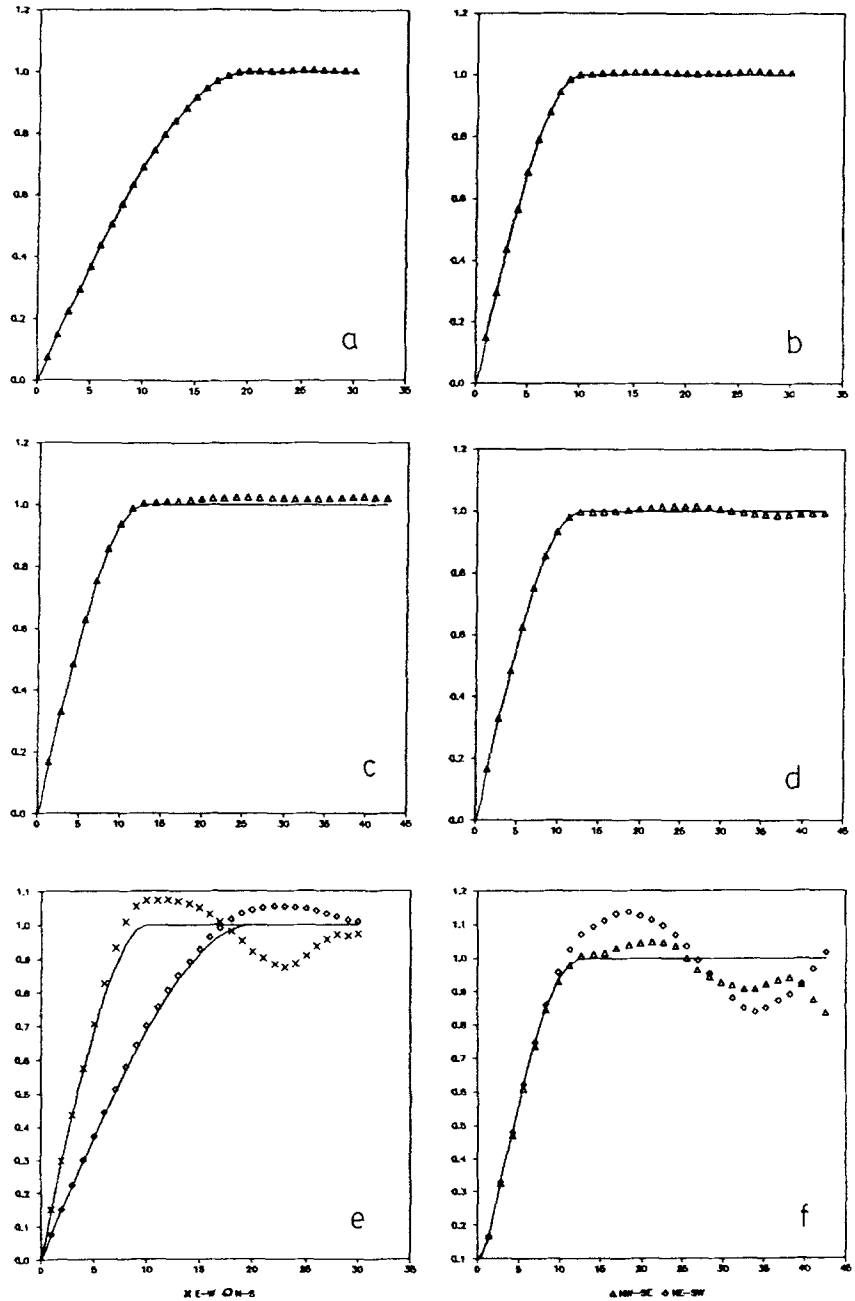

Fig. 18. Results of the FIM in 2D when the covariance has a geometric anisotropy. Average variogram of 100 realizations for directions (a) N-S, (b) E-W, (c) NE-SW, (d) NW-SE. Experimental variogram of a single random realization for directions: (e) X axis: distance, Y axis: variogram function. ——: model, Δ, o, x: simulation.

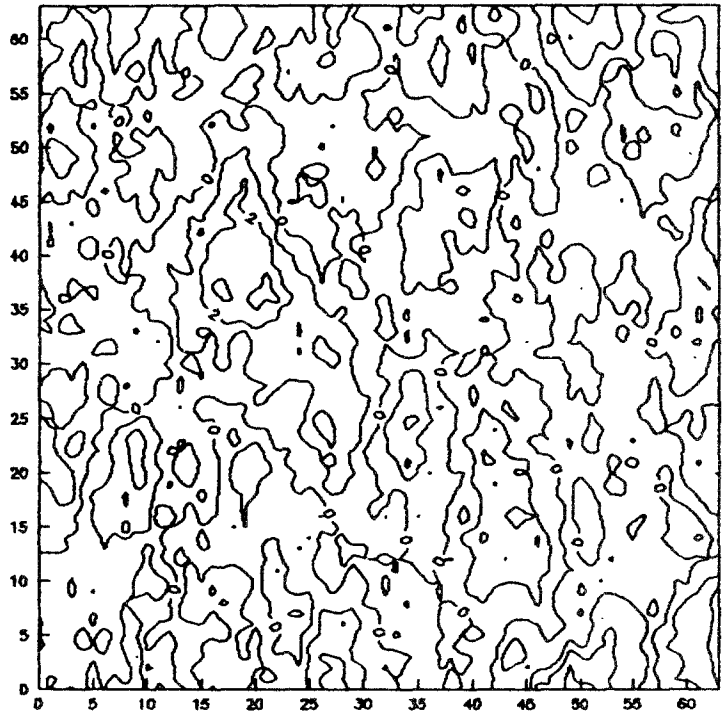

Fig. 19. Cartography of a single realization with geometric anisotropy. X axis: distance, Y axis: distance.

dom field. Let a random field to be a two-dimensional random function with geometric and zonal anisotropy in the X-Y plane. For example, we consider the model:

$$C(x, y) = C_x \left[1 - \frac{3}{2}\frac{x}{a_x} + \frac{1}{2}\frac{x^3}{a_x^3} \right] + C_y \left[1 - \frac{3}{2}\frac{y}{a_y} + \frac{1}{2}\frac{y^3}{a_y^3} \right]$$

$a_x = 15$: range in the N-S direction (X axis), $a_y = 10$: range in the E-W direction (Y axis), $C_x = 0.7$: sill in the X direction, and $C_y = 0.3$: sill in the Y direction.

Figure 22 shows the results of the simulation. A good fit between the theoretical and simulated variogram is observed when ensemble values are considered. When only a single realization is considered discrepancies between the model and experimental variogram are greater (as was expected) mainly in the directions of anisotropy (N-S and E-W) because, as can be seen in Fig. 17b, when a zonal anisotropy is present in these directions, the spectral density decays to zero more slowly than in other directions and aliasing can be suspected. Better results can be obtained by increasing the size of the field to simulate.

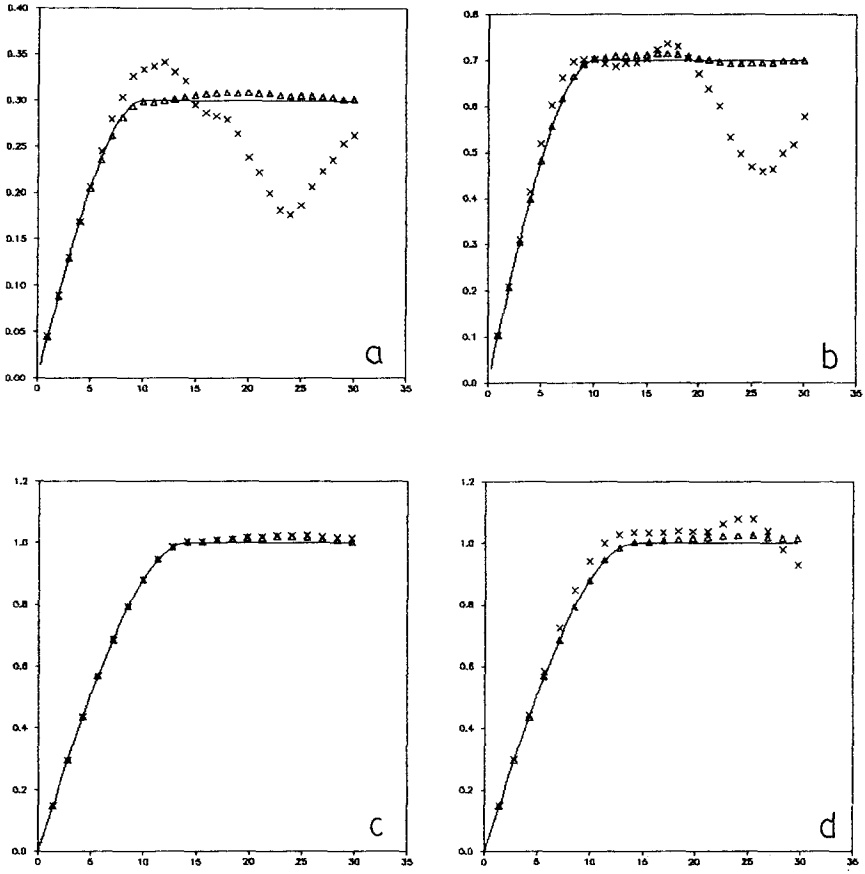

Fig. 20. Results of the FIM in 2D when the covariance has a zonal anisotropy. Directional variograms (a) N-S, (b) E-W, (c) NE-SW, (d) NW-SE. Δ: Average variogram of 100 realizations. *x*: Variogram of a single realization ——: model. *X* axis: distance, *Y* axis: variogram function.

The great similarity between Figs. 20a and 22a is because the two realizations are the same random phase spectrum and the only difference is the range in the *X* direction of the second example.

CONCLUSIONS

In this paper, the Fourier integral method (FIM) is presented as an efficient methodology for the generation of realizations of random functions in 1D, 2D, and 3D. Its main advantages with regard to the Turning Bands Method (TBM) are its generality to simulate any permissible covariance model and its good

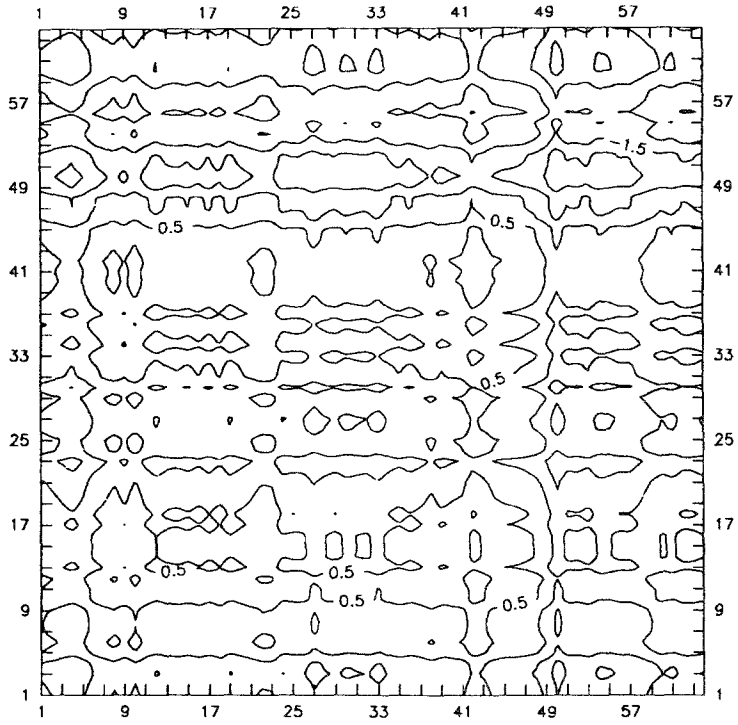

Fig. 21. Cartography of a single realization with zonal anisotropy. *X* axis: distance, *Y* axis: distance.

precision, shown by the behavior of the ensemble statistics and a lower coefficient of variation of the average variogram than that obtained by the TBM.

Moreover, the generation of realizations with nugget effect, nested structures and with anisotropic covariance (geometric, zonal or both) is immediate and no require any additional work. In 1D the method is also competitive with regard to the Shinozuka and Jand method mainly concerning the periodicity of the variogram simulated.

Its principal limitations, generation of points in a regular network and number of points on the axes to the power of two, can be solved easily in practice. On the other hand the method is highly competitive in computing time.

ACKNOWLEDGMENTS

The work in this paper was supported by the Dirección General de Investigación Científica y Técnica (DGICTYT) under Grant PB89-0015 and by the Grupo de Investigación de la Junta de Andalucia n° 4020. We would like to thank both the anonymous referees for their invaluable constructive comments.

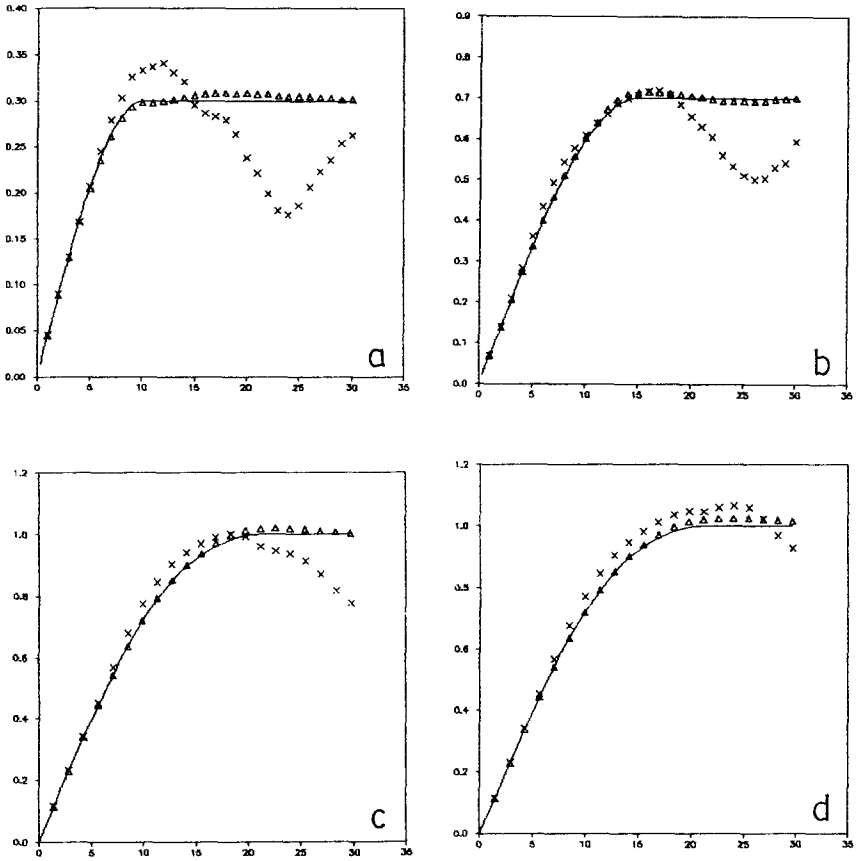

Fig. 22. Results of the FIM in 2D when the covariance has both geometric and zonal anitotropy. Directional variograms: (a) N-S, (b) E-W, (c) NE-SW, (d) NW-SE. Δ: Average variogram of 100 realizations. *x*: Variogram of a single realization. ——: model. *X* axis: distance, *Y* axis: variogram function.

REFERENCES

Anderson, T. W., 1971, The Statistical Analysis of Times Series: John Wiley and Sons, New York, p. 704.

Black, T. C., and Freyberg, D. L., 1990, Simulation of One-Dimensional Correlated Fields Using a Matrix-Factorization Moving Average Approach: Math. Geol., v. 22, p. 39–62.

Borgman, L., Taheri, M., and Hagan, R., 1984, Three-Dimensional Frequency-Domain Simulations of Geological Variables: Proc. NATO ASI, Lake Tahoe, Sept. 1983, p. 517–541.

Bracewell, R. N., 1986, The Fourier Transform and Its Applications: Mc-Graw Hill International Editions, Singapore, p. 474.

Brigham, E. O., 1988, The Fast Fourier Transform and Its Applications: Prentice-Hall International Editions, London, p. 448.

Brooker, P. I., 1985, Two-Dimensional Simulation by Turning Bands: Math. Geol., v. 17, p. 81–90.

Chatfield, C., 1991, The Analysis of Time Series, 4th ed.: Chapman and Hall, London, p. 241.

Christakos, G., 1987, Stochastic Simulation of Spatially Correlated Geo-Processes: Math. Geol., v. 19, p. 807–831.

Cox, D. R., and Miller, H. D., 1968, The Theory of Stochastic Processes: Methuen & Co. Ltd., London, p. 397.

Dowd, P., 1991, A Review of Recent Developments in Geostatistics: Comp. Geosci., v. 17, p. 1481–1500.

Fox, G. C., 1987, An Inverse Fourier Transform Algorithm for Generating Random Signals of a Specified Spectral Form: Comp. Geosci., v. 13, p. 369–374.

Hsu, H. P., and Mehra, R., 1973, Análisis de Fourier: McGraw Hill, Bogotá, p. 274.

Isaaks, E. H., and Srisvastava, R. M., 1989, Applied Geostatistics: Oxford University Press, New York, p. 561.

Journel, A., 1974, Geostatistics for Conditional Simulation of Ore Bodies: Econ. Geol., v. 69, p. 673–687.

Journel, A., and Huijbregts, C., 1978, Mining Geostatistics: Academic Press, New York, p. 600.

Mantoglou, A., 1987, Digital Simulation of Multivariate Two- and Three-Dimensional Stochastic Processes with a Spectral Turning Bands Method: Math. Geol., v. 19, p. 129–149.

Mantoglou, A., and Wilson, J. L., 1982, The Turning Band Method for Simulation of Random Fields Using Line Generation by a Spectral Method: Water Res. Res., v. 18, p. 1379–1394.

Matheron, G., 1973, The Intrinsic Random Functions and Their Applications: Adv. Appl. Prob., v. 5, p. 439–468.

Pardo-Igúzquiza, E., 1991, Simulación Geoestadística de Variables Geológicas por Métodos Espectrales. Ph.D. Thesis, Department of Geodynamics, University of Granada, p. 412.

Schrage, L., 1979, A More Portable Fortran Random Number Generator: ACM Trans. Math. Soft., v. 5, n. 2, p. 132–138.

Shinozuka, M., and Jan, C. M., 1972, Digital Simulation of Random Processes and Its Applications: J. Sound Vibr., v. 25, p. 111–128.

Weaver, H. J., 1989, Theory of Discrete and Continuous Fourier Analysis: John Wiley and Sons, New York, p. 307.